Lawrence Berkeley Laboratory
UNIVERSITY OF CALIFORNIA

Materials & Molecular Research Division

Submitted to Progress in Nuclear Energy

THE THEORY OF URANIUM ENRICHMENT BY THE GAS CENTRIFUGE

Donald R. Olander

March 1981

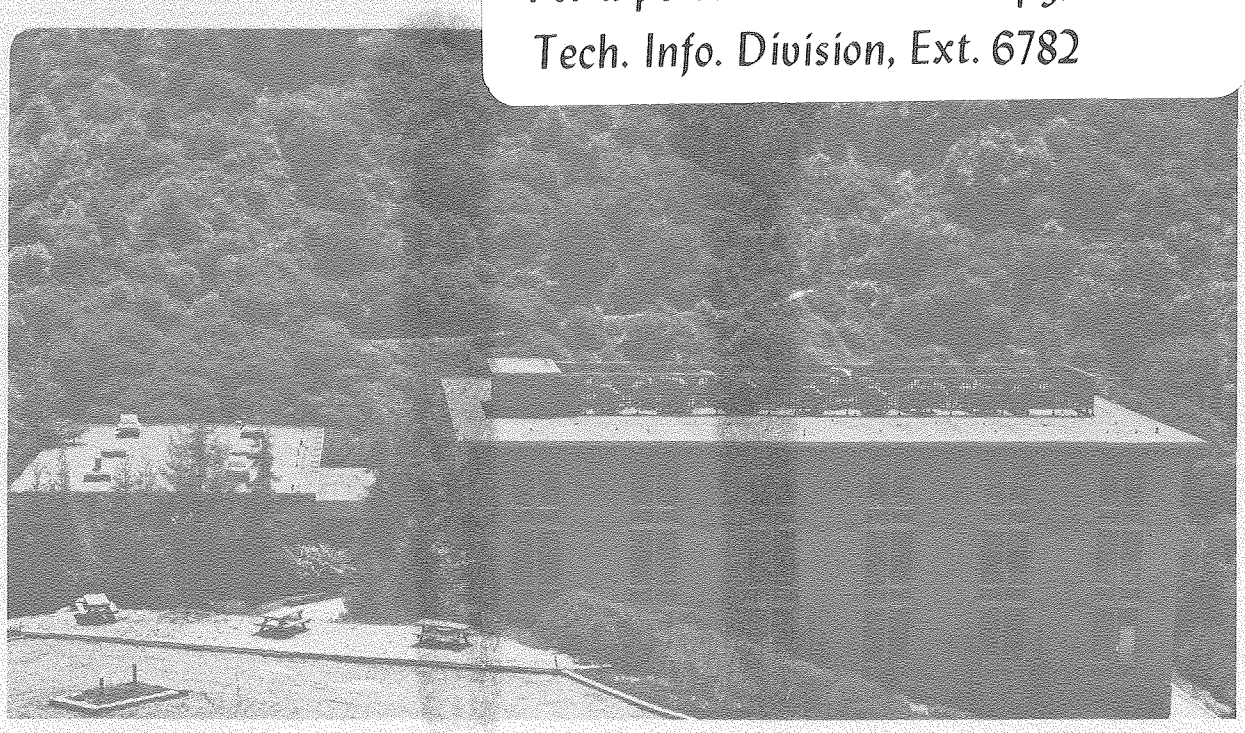

Prepared for the U.S. Department of Energy under Contract W-7405-ENG-48

DISCLAIMER

LBL-10253
March 1981

THE THEORY OF URANIUM ENRICHMENT BY THE GAS CENTRIFUGE

by Donald R. Olander

Materials and Molecular Research Division of the Lawrence Berkeley Laboratory and the Department of Nuclear Engineering University of California, Berkeley, California 94720

ABSTRACT

Onsager's analysis of the hydrodynamics of fluid circulation in the boundary layer on the rotor wall of a gas centrifuge is reviewed. The description of the flow in the boundary layers on the top and bottom end caps due to Carrier and Maslen is summarized. The method developed by Wood and Morton of coupling the flow models in the rotor wall and end cap boundary layers to complete the hydrodynamic analysis of the centrifuge is presented. Mechanical and thermal methods of driving the internal gas circulation are described. The isotope enrichment which results from the superposition of the elementary separation effect due to the centrifugal field in the gas and its internal circulation is analyzed by the Onsager-Cohen theory. The performance function representing the optimized separative power of a centrifuge as a function of throughput and cut is calculated for several simplified internal flow models. The use of asymmetric ideal cascades to exploit the distinctive features of centrifuge performance functions is illustrated.

This work was supported by the Director, Office of Energy Research, Office of Basic Energy Sciences, Materials Sciences Division of the U.S. Department of Energy under Contract Number W-7405-ENG-48.

A. INTRODUCTION

Uranium enrichment is an essential component of nuclear fuel cycles based upon light water reactors. For more than thirty years, the uranium enrichment industry has been based solely on gaseous diffusion technology. Because of the substantial electrical power requirements of this process, the gas centrifuge method, which requires only about 5% of the power for comparable enrichment, has been selected for most additional capacity. The early theoretical work on the gas centrifuge is presented in the book by Cohen[1]. The recent books by Avery and Davies[2], Villani[3] and Benedict and al[4] provide more up-to-date discussions, and Soubbaramayer[5] has summarized the current status of non-U.S. theoretical work. Summaries of early hydrodynamic analyses and separation theory are presented in ref.[6] and a semi-technical description of the device is given in ref.[7].

There are many reasons for engaging in theoretical analysis of a gas centrifuge. First, such calculations can be used to guide experiments, which for a fully-instrumented test machine, are quite costly. Second, they provide an understanding of how the flow affects isotope separation and may suggest means of altering the flow profiles to improve performance. Third, they permit an assessment of off-optimum performance of the centrifuge. Finally, they can be used in engineering cost optimization studies, the object of which is to design a machine and operate it so that the cost per unit of separative power is a minimum. This last feature of the theory is especially important, because the large number of parameters controlling the internal flow (and hence the separation) makes experimental optimization expensive and tedious. Because of the large scale of the uranium enrichment industry, even a few percent improvement in a separative power of a device (at no expense) means yearly saving of many millions of dollars in the cost of electricity generated by light water reactors.

Figure 1 shows an early gas centrifuge. The current models are of the same general type but are larger and are capable of much higher speeds.

Machines with diameters as large as 24 inches have been tested. Figure 2 is a schematic of the centrifuge. An electric motor resting on the bottom of the casing turns a shaft attached to the bottom of the rotor, into which UF_6 gas is fed at about the mid-point of the stationary post on the axis. In addition to the feed tube, this post also contains conduits for removing the enriched product and the depleted waste streams from the machine. The rotor is centered by the bearing assembly on top, where contact between moving and stationary parts is avoided by magnetic alignment. The space between the spinning rotor and the outer casing is evacuated by a diffusion pump.

The vertical arrows inside the rotor of Fig. 2 represent the internal gas circulation which is in large part responsible for the favorable separative properties of the centrifuge. This countercurrent flow can be "driven" in a variety of ways. The term "drive" connotes a means of generating the internal circulation in the rotor; "thermal drive" is accomplished by controlling the rotor wall or end cap temperatures; "mechanical drive" is achieved by causing the rotating as to interact with stationary objects inside the rotor. The circulation patterns generated by the various driving mechanisms can be analyzed individually and their flow contributions added together to give the total hydrodynamic velocity. This separability feature arises because the state of the flow is only slightly perturbed from the primary wheel flow (i.e. solid body rotation) so that the equations of motion can be linearized.

The important driving mechanisms are :

1. Wall thermal drive, which is generated by a nonuniform temperature distribution along the length of the rotor wall. To obtain the direction of gas circulation in the same sense as that produced by the principal mechanical drive, the rotor wall temperature decreases from bottom to top.

2. End cap thermal drive results from removing heat from the top end of the rotor or adding heat through the bottom end cap.

3. Feed drive is the gas circulation induced by injection of the feed stream at or near the middle of the rotor.

4. Scoop drive is the main mechanical drive. It refers to the flow developed by the interaction of the stationary bottom scoop with the spinning gas.

The magnitudes of each of these contributions to the total internal circulation can be adjusted by experimentally controllable parameters. Wall thermal drive is directly proportional to the longitudinal temperature gradient along the rotor wall. End cap thermal drive is directly proportional to the difference in temperature between the bottom plate and the gas adjacent to it and to the corresponding difference at the top end cap (or more precisely, at the rotating baffle in Fig. 2). Figure 3 shows the boundary temperature profiles which generate the two types of thermal drives.

In addition to a net upflow (product rate) in the enriching section, feed introduction produces a gas flow pattern which is labelled feed drive. The magnitude of this component of the countercurrent is proportional to the machine throughput, or the feed rate.

Scoop drive is controlled by the radial location of the waste scoop tip in the "atmosphere" of gas attached to the rotor wall and by the size and shape of the scoop. The top scoop is shielded from the main gas flow by the rotating baffle ; without this baffle, the top scoop would generate a countercurrent opposing the one produced by the bottom scoop.

The flow patterns arising from each of these drives can be theoretically modeled independently of the others. The total circulation rate is the sum of the contributions due to the four driving mechanisms. In particular, the axial mass velocity is the crucial aspect of the hydrodynamics needed for separation theory, and can be written as :

$$\rho w = (\rho w)_W + (\rho w)_F + (\rho w)_S + (\rho w)_E \qquad (1)$$

where w is the axial component of the fluid velocity and ρ is the gas density, which is primarily a function of radial position. The product of the axial velocity and the density is the axial mass flow rate per unit area. The subscripts w, E, F and S refer to wall thermal, end cap thermal, feed and scoop drives, respectively. Each of these components has a distinct radial shape and axial variation, and the magnitude of each is controllable by the experimental parameters mentioned previously. The flow profile in the centrifuge can be "fine tuned" for maximum separative performance by manipulation of the variables controlling the drives.

The density of the gas at the rotor wall, ρ_w, is also a controllable parameter of the centrifuge. It can be varied by adjusting the size, number, and positions of the holes in the rotating baffle which removes product (Fig. 2) and by the position and size of the opening of the bottom scoop which removes the depleted gas. These structural features, when combined with downstream valves, fix the conductances of the exit lines. The rate of outflow from the centrifuge is proportional to the product of the gas pressure at the wall p_w, (or to the density ρ_w) and the conductances of the lines. Thus, by adjusting the conductances of the exit lines and specifying the feed rate, the gas density at the rotor wall can be controlled. The cut, equal to the product rate divided by the throughput, is also adjusted in this manner.

As will be shown in section C, the aspect of the hydrodynamics which enters separation theory is the <u>flow function</u>, defined by:

$$F(r, z) = 2\pi \int_0^r \rho_w \; (r', z)\; r'\, dr' \qquad (2)$$

where r and z denote radial and axial positions in the rotor. $z = 0$ is the bottom (waste) end of the centrifuge and the product is removed at $z = Z$, the rotor height. The flow function can also be broken down into

components representing the basic drives :

$$F = F_w + F_E + F_F + F_S \qquad (3)$$

Each of the terms on the right hand side of Eq (3) is of the form of Eq (2) with the appropriate mass velocity in the integrand.

Early hydrodynamic analyses of the gas centrifuge[6] produced primarily solutions for ρw (or F) which did not change axially (i.e., "long-bowl" solutions). However, both the radial shape and the magnitude of the axial velocity are strongly dependent upon z, and the dependence on z of each of the drives is different. For example, wall thermal drive can be used to induce circulation in a centrifuge operated at total reflux (i.e., no feed, product or waste). In this case, flow vanishes at the top and bottom of the rotor and is largest at the midplane of the rotor. The scoop and end cap thermal drives on the other hand, are largest at the end where generation occurs and decay towards the opposite end.

While the hydrodynamics can be linearized, the separation calculation cannot. It is not possible to compute increments of separative power due to the various drives and add the increments together to obtain the total separative power; the total flow function represented by the left hand side of Eq. (3) must be used in the separative analysis.

B. HYDRODYNAMICS

B.1. Perturbations from the Equilibrium State

The physics of the gas centrifuge is contained in the equations of mass, energy and species conservation which govern the processes occurring in the gas within spinning rotor. Since the hydrodynamic equations may be decoupled from the species conservation (or diffusion) equation, it is convenient to divide the theoretical analysis into two parts. The first is the hydrodynamic analysis in which the gas is considered as a single component fluid. Simultaneous solution of the mass, momentum and energy

equations in conjunction with a thermodynamic equation of state provides the velocity profiles which are needed to solve the diffusion-convection equation. The second part is the separative analysis, which explicity treats the gas as a two-component mixture. This step requires solution of the diffusion-convection equation and is considered in Section C.

In the absence of thermal or mechanical perturbations of the gas in the rotor, a state of thermodynamic equilibrium is achieved. The gas rotates as a rigid body and is characterized by the following properties[4,5]:

$$V_{\theta eq} = \Omega r, \quad V_{zeq} = 0, \quad V_{req} = 0$$
$$\rho_{eq}/\rho_w = p_{eq}/p_w = \exp\left\{-A^2\left[1-\frac{r^2}{a^2}\right]\right\}, \quad T_{eq} = T_o \tag{4}$$

where V_z, V_r and V_θ are the components of velocity in the axial, radial, and azimuthal directions, and p, ρ, and T denote the thermodynamic variables pressure, mass density, and temperature. The subscript "eq" indicates equilibrium conditions, Ω is the angular velocity of the rotor, a is the rotor radius, and T_o is the temperature of the gas. The dimensionless quantity A is defined by

$$A^2 = \frac{M\Omega^2 a^2}{2RT_o} \tag{5}$$

where R is the gas constant and M is the molecular weight. The quantity A is the ratio of the peripheral speed (Ω a) to the most probable molecular speed $\sqrt{2RT_o/M}$ of the gas; it is approximately equal to the Mach number of the rotor wall and is typically in the range 5-6.

The flow field becomes much more complex when circulation currents are generated by one or more of the driving mechanisms discussed in Section A. In addition to the convection established in the stratified gas next to the rotor wall, flow along the solid caps at the axial extremeties of the rotating

cylinder must be considered. Fortunately, two aspects of the nonequilibrium flow lead to simplifications which permit solution of the equations of motion.

First, the deviations of the velocity components and the thermodynamics state variables from the equilibrium solution of Eq. (4) are small enough to be treated as perturbations. Thus :

$$V_r = 0 + u \; ; \; V_\theta = \Omega r + v \; ; \; V_z = 0 + w$$
$$p = p_{eq} + \bar{p} \; ; \; \rho = \rho_{eq} + \bar{\rho} \; ; \; T = T_o + \bar{T} \qquad (6)$$

The nonlinear set of conservation equations (mass, momentum and energy) can be linearized about the equilibrium solution (Eq. (4)) and the resulting equations contain the perturbations u, v, w, $\bar{p}$, $\bar{\rho}$, and $\bar{T}$ to first order only. The linearized euqtions are:

Overall mass continuity :

$$\frac{1}{r}\frac{\partial}{\partial r}(\rho_{eq} r u) + \frac{\partial}{\partial z}(\rho_{eq} w) = 0, \qquad (7\text{ a})$$

Radial momentum:

$$-\bar{\rho} r\Omega^2 - 2\rho_{eq}\Omega v = -\frac{\partial \bar{p}}{\partial r} + \mu\left\{\frac{\partial}{\partial r}\left[\frac{1}{r}\frac{\partial}{\partial r}(ru)\right] + \frac{\partial^2 u}{\partial z^2}\right\}, \qquad (7\text{ b})$$

Angular momentum:

$$2\rho_{eq}\Omega u = \mu\left\{\frac{\partial}{\partial r}\left[\frac{1}{r}\frac{\partial}{\partial r}(rv)\right] + \frac{\partial^2 v}{\partial z^2}\right\}, \qquad (7\text{ c})$$

Axial momentum:

$$0 = -\frac{\partial \bar{p}}{\partial z} + \mu\left\{\frac{1}{r}\frac{\partial}{\partial r}\left(r\frac{\partial w}{\partial r}\right) + \frac{\partial^2 w}{\partial z^2}\right\}, \qquad (7\text{ d})$$

Energy:

$$-\rho_{eq}\Omega^2 r u = \kappa\left[\frac{1}{r}\frac{\partial}{\partial r}\left(r\frac{\partial \bar{T}}{\partial r}\right) + \frac{\partial^2 \bar{T}}{\partial z^2}\right], \qquad (7\text{ e})$$

Equation of state :

$$\bar{\rho} = \left(\frac{M}{RT_o}\right)\bar{p} - \rho_{eq}\left(\frac{\bar{T}}{T_o}\right) \qquad (7\text{ f})$$

The physical phenomena which are responsible for driving the internal circulation in the rotor are contained in the terms on the left hand sides of the radial and angular momentum equations and in the energy equation. The left hand side of Eq (7 b) represents the centrifugal force on the gas. The left hand side of Eq (7 c) is the Coriolis force. The left hand side of Eq (7 e) represents the reversible work done on the gas due to compression or expansion.

Second, only regions next to solid boundaries contain gas at significant density. The gas attached to the top and bottom end caps flows primarily in the radial direction and forms boundary layers often called the Ekman layers. The gas held close to the rotor wall by the strong centrifugal force flows in an axial countercurrent. This circulation is also of the boundary layer type and is sometimes termed the Stewartson layer because it is the compressible analog of the flow first investigated by this author [8]. Actually there are several different kinds of Stewartson layers, depending on the flow-driving mechanism[5]. In this review, the boundary layer formed by gas flow next to the vertical cylindrical wall of the centrifuge will be called the Stewartson layer.

The inner boundaries of the Ekman and Stewartson layers are not distinct. Rather, the flow decays exponentially with distance from the solid boundary. The characteristic thickness in the Ekman layers depends upon a dimensionless group called the Ekman number:

$$\varepsilon = \frac{\mu}{\rho_w \Omega a^2} \tag{8}$$

which is a reciprocal Reynolds number.

According to Eq. (4) the gas on the rotor wall in confined to a thin layer by the centrifugal force. Thus, the characteristic scaling parameter for the mass of gas in this layer is the quantity A^2 of Eq. (5), and the velocity perturbations extend radially inward only a fraction of the rotor radius.

The two types of boundary layer flows in the rotor are analyzed by different simplifications of the linearized equations of motion. In the Ekman layers, radial derivatives are small compared to axial derivatives, whereas in the Stewartson layer, the reverse is true. However, the flow in the vertical (Stewartson) and horizontal (Ekman) boundary layers must be properly matched in order to completely describe the circulation pattern in the rotor.

B.2. Onsager's Equation for Flow Near the Rotor Wall

Onsager[9] demonstrated that the linearized conservation equations can be reduced to a single sixth-order partial differential equation which describes the countercurrent flow in the Stewartson layer. Onsager's method is described in detail in a paper by Wood and Morton[10] and is summarized in Appendix A. Onsager's method of combining Eqs. (7a) through (7f) yields:

$$\frac{\partial^2}{\partial \xi^2}\left\{ e^{\xi} \frac{\partial^2}{\partial \xi^2}\left(e^{\xi} \frac{\partial^2 \chi}{\partial \xi^2} \right) \right\} + B^2 \frac{\partial^2 \chi}{\partial \eta^2} = 0 \qquad (9)$$

Radial position has been nondimensionalized by introducing the scale height variable:

$$\xi = A^2 \left(1 - \frac{r^2}{a^2} \right) \qquad (10)$$

where A^2 is given by Eq. (5) . The scale height variable is analogous to the altitude above the earth's surface. "Sea level" is the rotor wall and the density of the "atmosphere" of gas in the Stewartson layer decreases exponentially in ξ :

$$\rho_{eq} = \rho_w e^{-\xi} \qquad (11)$$

In arriving at Eq. (9), the ratio ξ/A^2 was neglected compared to unity. For large A this is acceptable since most of the gas is very close to the rotor wall. This simplification is known as the "pancake" approximation[10].

Axial position has been nondimensionalized by the rotor height Z:

$$\eta = z/Z \tag{12}$$

The dimensionless group B is given by:

$$B^2 = \frac{S}{16\, A^{12}\, \varepsilon^2\, (Z/a)^2} \tag{13}$$

where ε is the Ekman number defined by Eq. (8) and

$$S = 1 + A^2 Pr\ \frac{\gamma - 1}{2\gamma} \tag{14}$$

is a quantity which contains the gas transport properties as the Prandtl number ($Pr = \mu C_p/\kappa M$) and the specific heat ratio γ.

The quantity χ in Eq. (9) is Onsager's Master potential. It has dimensions of g-cm^2/sec, and can be nondimensionalized, if desired, by $\rho_w \Omega\, a^5$. The Master potential is related to the axial mass velocity by:

$$\rho_{eq}^{\ w} = \frac{4\, A^4}{a^4} \left(\frac{\partial^2 \chi}{\partial \xi^2}\right) \tag{15}$$

Using Eq. (2), the flow function is:

$$\frac{F - P}{2\pi} = -\frac{2A^2}{a^2} \frac{\partial \chi}{\partial \xi} \tag{16a}$$

in the enriching section and

$$\frac{F + W}{2\pi} = -\frac{2A^2}{a^2} \frac{\partial \chi}{\partial \xi} \tag{16b}$$

in the stripping section. In these equations, P and W are the product and waste flow rates, respectively, from the centrifuge.

B.3. Radial boundary conditions

Equation (9) requires axial boundary conditions at the top and bottom of the centrifuge, which will be considered in Sect. B.4, and six radial boundary conditions. Of the latter, three apply at the rotor wall and three prescribe the gas behaviour at the inner edge of the Stewartson layer.

Rotor wall conditions

i) the condition that the rotor wall be impermeable to the gas requires the radial velocity component u to vanish along the wall. This requirement and Eq. (A-14) of Appendix A provide the following condition on the Master potential:

$$\left(\frac{\partial \chi}{\partial \xi}\right)_{\xi = 0} = 0 \tag{17}$$

ii) the condition of no-slip at the rotor wall requires w = 0 at r = a, or, from Eq. (A-15), of Appendix A:

$$\left(\frac{\partial^2 \chi}{\partial \xi^2}\right)_{\xi = 0} = 0 \tag{18}$$

iii) the final wall boundary condition is provided by specification of the rotor wall temperature perturbation, $\overline{T}_w(z) = T_w(z) - T_o$, where $T_w(z)$ is the applied temperature distribution on the wall (e.g., Fig. 3b). It is not possible to control the temperature of the inner wall of the rotor directly. All that can be done in a practical sense is to provide a controlled heat source in the vacuum of the casing just outside of the rotating cylinder. The thermal boundary condition is then determined by a heat transfer analysis involving the axial variation of the heat flux from the source, the thermal resistance due to radiant heat transfer from the heat source to the outside of the rotor wall, conduction through the wall, and convective transfer from the inner wall to the gas in the rotor. This condition is replaced by one approximating the temperature perturbation

along the inner wall by a quadratic function of axial position, which, besides considerably simplifying the theory, is probably sufficient for the practical purposes. Thus:

$$\frac{\bar{T}_w}{T_o} = \text{constant} + q'\eta + \frac{1}{2} q'' \eta^2 \qquad (19)$$

where q' and q'' are specified constants.

In the theory developed in Appendix A, the temperature perturbation $\bar{T}$ and the azimuthal velocity perturbation v appear as the combined parameter:

$$\Phi = \frac{\bar{T}}{T_o} - \frac{2v}{\Omega r} \qquad (20)$$

This quantity is related to the Master potential by Eq. (A-16) of Appendix A which, in terms of the dimensionless position variables and after one radial integration, provides the following condition:

$$\left(\frac{\partial \Phi}{\partial \eta}\right)_{\xi=0} = \frac{32 (Z/a) A^{10} \varepsilon}{\rho_w \Omega a^5} \left(L_5 \chi\right)_{\xi=0}$$

where L_5 is the fifth order operator :

$$L_5 = \frac{\partial}{\partial \xi}\left[e^{\xi} \frac{\partial^2}{\partial \xi^2}\left(e^{\xi} \frac{\partial^2}{\partial \xi^2} \right)\right] \qquad (21)$$

Evaluating $(\partial \Phi / \partial \eta)_{\xi=0}$ from Eqs (19) and (20), and noting that the no-slip condition requires that v = 0 at the wall, the temperature distribution along the length of the rotor gives the boundary condition :

$$\left(L_5 \chi\right)_{\xi=0} = \frac{\rho_w \Omega a^5}{32 (Z/a) A^{10} \varepsilon} (q' + q'' \eta) \qquad (22)$$

Conditions at the Inner boundary of the Stewartson layer

The inner boundary of the Stewartson layer, or the "top of the atmosphere", corresponds roughly to the demarcation between the continuum flow regime which characterizes the dense gas attached to the rotor wall and the regime of rarefied gas flow in the centrifuge core. The inner boundary is defined as that radial position (ξ_o) where the mean free path of the gas molecules is equal to a distance corresponding to a unit of scale height. From Eq (10), a unit scale height increment corresponds to a distance of $a/2A^2$ for positions close to the rotor wall. The mean free path is :

$$\lambda = \frac{M}{\sqrt{2}\,\pi\sigma^2\rho_o N_{av}} = \frac{M\cdot e^{\xi_o}}{\sqrt{2}\,\pi\sigma^2\rho_w N_{av}}$$

where σ is the molecular diameter of UF_6, N_{av} is Avogadro's number and ρ_o is the gas density at the top of the atmosphere, given by Eq. (11) at $\xi = \xi_o$. Setting $\lambda = a/2A^2$, the inner boundary of the Stewartson layer is determined by :

$$\xi_o = \ln\left[\frac{\pi\sigma^2 N_{av}\rho_w a}{\sqrt{2}\,A^2 M}\right] \qquad (23)$$

Taking $\sigma = 4$ Å and typical values of the other quantities in this formula, we find ξ_o is in the range 8-10. In practice, the computed velocity field is not sensitive to the numerical value of ξ_o as long as it is larger than the value given by Eq (23).

Because of the exponential variation of density with distance from the wall, the fraction of the gas contained in the annular ring between the wall and the top of the atmosphere is $1 - e^{-\xi_o}$. The location defined by Eq (23) thus contains more than 99.9 % of the gas in the rotor. The radial location of the top of the atmosphere depends

upon the peripherial speed which is contained in A^2 in Eq. (10). For high-speed centrifuges, $\xi_o = 8$ corresponds to a radial location greater than 80% of the radius of the bowl.

The Onsager method completely disregards the behavior of the small quantity of gas in the inside of the centrifuge. This represents a significant difference from the approach followed by European and Japanese workers [5], who explicitly treat gas flow in the core and match the inner flow to that in the Stewartson layer. The Onsager approach thus provides a significant simplification in the analysis.

iv) Feed is introduced into the centrifuge through holes or slots in the central post near the midplane (Fig. 2). The gas moves from the feed port in free-molecule flow and begins to interact appreciably with the circulating gas in the Stewartson layer (via molecular collisions) at the radial position ξ_o just calculated. Although the feed enters the circulating flow with an axial spread on the order of a rotor diameter above and below the axial location of the feed port on the post, we neglect this spread and assume that the injected gas constitutes a circular line source of L mass units per unit time (the feed rate to the centrifuge) at specified height η_F and radial location r_o, which corresponds to the scale height ξ_o. The input rate L is divided into a net upflow rate P and a net downflow rate W, according to the cut at which the centrifuge is set to operate. These net flows are related to the axial velocity by:

$$2\pi \int_{r_o}^{a} \rho_{eq}\, w r dr = \begin{cases} P & \text{for} \quad 0 \le \eta \le \eta_F \\ -W & \text{for} \quad \eta_F \le \eta \le 1 \end{cases} \tag{24}$$

Expressing the left hand side in terms of the Master potential by Eqs. (A-12) and (A-13) of Appendix A, the boundary condition representing feed introduction is:

$$\left(\frac{\partial \chi}{\partial \xi}\right)_{\xi = \xi_o} = \begin{cases} \dfrac{a^2 P}{4\pi A^2} & \text{for} \quad 0 \le \eta \le \eta_F \\ -\dfrac{a^2 W}{4\pi A^2} & \text{for} \quad \eta_F \le \eta \le 1 \end{cases} \tag{25}$$

v) As a second boundary condition at the inner edge of the Stewartson layer, the axial velocity is required to have no radial gradient at this point. Using Eqs. (A-15) and (11), this requirement supplies the relation:

$$\left[\frac{\partial}{\partial \xi}\left(e^{\xi}\ \frac{\partial^2 \chi}{\partial \xi^2}\right)\right]_{\xi=\xi_0} = 0 \qquad (26)$$

vi) Similarly, the radial gradients of the temperature and the azimuthal velocity perturbations are assumed to vanish at the top of the atmosphere. By virtue of Eq. (20), these two restrictions are combined into the single condition:

$$\left(\frac{\partial \Phi}{\partial \xi}\right)_{\xi=\xi_0} = 0$$

To relate this equation to the Master potential, we note that the right hand side of Eq. (A-16) can be expressed in terms of the axial derivative of χ by use of Eq. (A-24), from which we conclude, after one axial integration, that:

$$\frac{\partial \Phi}{\partial \xi} = \frac{-2S}{\varepsilon A^2}\ \frac{1}{\rho_w \Omega\ a^5}\ \frac{\partial \chi}{\partial \eta} \qquad (27)$$

Combining the preceding two equations, the final radial boundary condition is:

$$\left(\frac{\partial \chi}{\partial \eta}\right)_{\xi=\xi_0} = 0 \qquad (28)$$

The six radial boundary conditions on Onsager's Master equation are given by Eqs. (17), (18), (22), (25), (26) and (28). Equations (22) and (25) incorporate centrifuge flow drives due to rotor wall temperature nonuniformity and feed injection, respectively, subject to the restrictions discussed in connection with their development.

B.4. Solution of the Master Equation

There is an appreciable literature on the solution of the hydrodynamic

equations of a gas centrifuge by the method of separation of variables, or the eigenfunction expansion method. Early studies using this technique were reported by Parker and Mayo[11] and Ging[12]. Jacques[13] and Brouwers[14] have extended this approach. Onsager's Master equation, Eq. (9), is also amenable to solution by the eigenfunction expansion method[10]. The solution $\chi(\xi,\eta)$ is assumed to consist of a sum of terms of the separable form $f(\xi)\, h(\eta)$, thereby decomposing Eq. (9) into a pair of ordinary differential equations representing the radial and axial behavior of the Master potential:

$$\frac{d^2}{d\xi^2}\left\{ e^{\xi} \frac{d^2}{d\xi^2} \left(e^{\xi} \frac{d^2 f}{d\xi^2} \right) \right\} + \lambda^2 f = 0 \qquad (29)$$

and

$$\frac{d^2 h}{d\eta^2} - \frac{\lambda^2}{B^2} h = 0 \qquad (30)$$

where λ is the eigenvalue, which may be zero, real, or imaginary. Each of these cases gives rise to a particular axial function $h(\eta)$ and a distinct set of eigenfunctions $f(\xi)$. These are labeled as follows :

The zero eigenvalue modes correspond to $\lambda = 0$ and lead to axial solutions which are linear in η and to radial functions designated by $f^0(\xi)$. The corresponding product solution for the Master potential is denoted by χ^0.

The end modes result from solutions of Eqs (29) and (30) for real (and positive) values of λ. The axial shapes are exponential in η and the corresponding radial eigenfunctions are designated by $f^E(\xi)$. The Master potential obtained from the real eigenvalue solutions is denoted by χ^E.

The lateral modes arise from imaginary eigenvalues. These modes exhibit sinusoidal or cosinusoidal axial variations. This class of solutions is not considered here because, according to Wood and Morton[10], they are required only if the temperature distribution along the rotor

wall cannot be expressed by the quadratic form of Eq. (19), or if the feed distribution is more complicated than the delta function which leads to Eq. (25). Should the need arise, however, the lateral mode solutions are available[10].

With this restriction, the complete solution for the Master potential is expressed by:

$$\chi = \chi^0 + \chi^E \tag{31}$$

In this section, the general solutions for χ^0 and χ^E are summarized and the boundary conditions developed in the previous section are used to determine the constants of integration appearing in the general solutions.

Zero Eigenvalue Modes

These solutions were first obtained by Parker[15]. There are only three product solutions which contribute to χ^0:

$$\chi^0 = C_0\eta + (B_1+C_1\eta)f_1^0(\xi) + (B_2+C_2\eta)f_2^0(\xi) \tag{32}$$

where

$$f_1^0(\xi) = -2e^{-\xi} + (\frac{3}{2} + \xi)e^{-2\xi} \tag{33a}$$

$$f_2^0(\xi) = \frac{1}{2}\xi + e^{-\xi} - \frac{1}{4}e^{-2\xi} \tag{33b}$$

Substituting χ^0 of Eq. (32) into Eq. (28) and noting that $f_1^0(\xi_o) \simeq 0$ and $f_2^0(\xi_o) \simeq \xi_o/2$ (because exp $(-\xi_o)$ is very small), there results:

$$C_0 = -\frac{1}{2} C_2 \xi_o \tag{34}$$

The arbitrary definition of the inner boundary of the Stewartson layer by Eq (28) directly affects only the constant C_0. However, because the hydrodynamic quantities needed in the separative analysis [i.e., the axial speed or the flow functions in Eqs. (15) and (16)] involve only derivatives of the Master potential with respect to ξ, this uncertainly is of no practical consequence.

The second term on the right hand side of Eq (32) accounts for the rotor wall temperature distribution of Eq (19) via the boundary condition of Eq (22). Operating on $f_1^0(\xi)$ of Eq. (33a) by Eq. (21) gives $(L_5 f_1^0)_0 = 4$. Similar treatment of $f_2^0(\xi)$ of Eq (33b) yields $(L_5 f_2^0)_0 = 0$. Therefore, Eq (22) becomes :

$$4\,(B_1 + C_1\eta) = \frac{\rho_w \Omega\, a^5}{32\,(Z/a)A^{10}\,\varepsilon}\,(q' + q''\eta)$$

since this equation is valid for all η, we have :

$$B_1 = \frac{\rho_w \Omega\, a^5\, q'}{128(Z/a)A^{10}\,\varepsilon} \tag{35}$$

and

$$C_1 = \frac{\rho_w \Omega\, a^5\, q''}{128(Z/a)A^{10}\,\varepsilon} \tag{36}$$

Constant wall temperature gradient is a commonly treated case. In this situation $q'' = 0$ and

$$q' = \frac{1}{T_o}\,\frac{dT_w}{d\eta} \tag{37}$$

so that B_1 is proportional to the wall temperature gradient.

The last term on the right hand side of Eq. (32) accounts for the delta function type of internal feed to the centrifuge via the boundary condition of Eq. (25). Substituting Eq. (32) into the left hand side of Eq. (25) and noting from Eqs. (33a) and (33b) that $(df_1^0/d\,\xi)_{\xi_o} = 0$ and $(df_2^0/d\,\xi)_{\xi_o} = 1/2$ (again using the approximation $\exp(-\xi_o) \simeq 0$), we have:

$$\left(\frac{\partial \chi^0}{\partial \xi}\right)_{\xi=\xi_o} = \frac{1}{2}\,(B_2 + C_2 \eta) \tag{38}$$

The coefficients B_2 and C_2 can be obtained by combining Eq. (25) and (38):

$$B_2 = \begin{cases} \dfrac{a^2 P}{2\pi A^2} & \text{for } 0 \le \eta \le \eta_F \\ -\dfrac{a^2 W}{2\pi A^2} & \text{for } \eta_F \le \eta \le 1 \end{cases} \tag{39}$$

and

$$C_2 = 0 \tag{40}$$

This method was used by Parker[15].

Parker[15] and Wood and Morton[10] treat an additional zero eigenvalue solution, $(B_3+C_3\,\eta)\,(\xi\, e^{-\xi} + \frac{1}{2}\, e^{-2\xi})$, which is to be added to the right hand side of Eq. (32). However, this solution satisfies the boundary condition of Eq. (26) only if $B_3 = C_3 = 0$, and so need not be included in the analysis. The other solutions included in χ^0 of Eq. (32) automatically satisfy Eq. (26).

Thus, Eq. (32) is a solution of Onsager's Master equation which satisfies all of its radial boundary conditions with the constants given by Eqs. (34), (35), (36), (39) and (40). However, as shall be shown shortly, it is not the complete solution, even when no end drives are active.

End Modes

An additional solution of Onsager's Master equation is needed

in order to properly match the zero eigenvalue solution (if feed and/or wall thermal drive are active) to the Ekman layers at the top and bottom of the rotor. This additional solution, the end mode solution, also provides a means of incorporating scoop drive and end cap thermal drive into the analysis. The end mode solution was first deduced by Onsager [9]. The eigenfuctions and eigenvalues associated with this solution were computed by Morton [16] and the method of joining the end modes to the Ekman flow is discussed in detail by Wood and Morton [10]. In this section, we summarize the end mode solution. The method of coupling this solution to those for the Ekman layers is treated in a subsequent section.

The end modes represent solutions to the eigenfunction expansion of Onsager's Master equation wherein the eigenvalues λ are real and positive. The general solution of Eq. (30) for the axial dependence of the end modes is:

$$h^E = D \exp\left(-\frac{\lambda}{B}\eta\right) + E \exp\left[-\frac{\lambda}{B}(1-\eta)\right] \qquad (41)$$

which indicates exponential decay with distance from each end cap.

The radial shape of the end modes is determined by the eigenfunctions $f_n^E(\xi)$ and the eigenvalues λ_n obtained from the solution of Eq. (29) and the appropriate boundary conditions. The solution method due to Morton [10,16] is given in Appendix B. The first four end-mode eigenfunctions are shown in Fig. 4 along with their corresponding eigenvalues. These radial shape functions are the end-driven analogs of the zero eigenvalue modes whose radial dependence is given by the functions f_1^0 and f_2^0 of Eq. (33). It should be noted that the flow functions of interest in separation theory are proportional to the radial derivative of the Master potential [Eqs. (15) and (16)] and do not have the radial shape of the latter.

Combining the end mode eigenfunctions with the axial shape for the associated eigenvalue from Eq. (41) permits reconstruction of the Master potential component arising from the end modes:

$$\chi^E = \sum_{n=1}^{\infty} f_n^E(\xi)\left\{D_n \exp\left(-\frac{\lambda_n}{B}\eta\right) + E_n \exp\left[-\frac{\lambda_n}{B}(1-\eta)\right]\right\} \qquad (42)$$

Determination of the coefficients D_n and E_n requires matching the flow profile in the Stewartson layer to that in the Ekman layers, which is the subject of the following section.

B.5. Coupling of the Stewartson and Ekman layer solutions

The flow in the Ekman layers on the top and bottom end caps is important to the hydrodynamics analysis because it provides the mechanism by which the imposed end cap conditions are communicated to the main flow in the rotor. In effect, the Ekman layer analysis is a means of providing axial boundary conditions for the Onsager Master equation, and serves to determine the coefficients D_n and E_n in Eq. (42).

The analysis of the flow on the end caps given by Carrier and Maslen[17], which is summarized in Appendix C, leads to a relation involving the quantity ϕ of Eq. (20) and the stream function:

$$\Psi = \frac{1}{\rho_{eq}\,\Omega a^3} \int_r^a \rho_{eq}\, wr'\, dr' \tag{43}$$

Carrier and Maslen showed that the flow parameters ϕ and Ψ in the Stewartson layer at the bottom of the rotor (subscript ∞) are related to those on the bottom end cap (subscript B) by:

$$\phi_\infty - \phi_B = \frac{4\, S^{3/4}\, e^{-\xi/2}}{\sqrt{\varepsilon}} \left(\Psi_\infty - \Psi_B\right) \tag{44}$$

where ε and S are given by Eqs. (8) and (14), respectively.

A similar equation can be derived for the Ekman/Stewartson matching condition at the top end cap:

$$\phi_\infty - \phi_T = -\frac{4\, S^{3/4}\, e^{-\xi/2}}{\sqrt{\varepsilon}} \left(\Psi_\infty - \Psi_T\right) \tag{45}$$

where Ψ_T and ϕ_T are the specified, radially-dependent stream function and aximuthal velocity-temperature perturbation parameter on the top end

cap (actually at the rotating baffle in Fig. 2). Ψ_∞ and ϕ_∞ are the corresponding quantities in the upper end of the Stewartson layer where it meets the top Ekman layer.

In order to match the Ekman and Stewartson layers at the ends of the centrifuge, the stream function Ψ_∞ needs to be expressed in terms of the Master potential and Ψ_B and Ψ_T must be related to the method of gas extraction from the rotor. The features of this procedure at the bottom end cap are depicted in Fig. 5. For computational purposes, waste removal is simulated by flow of gas through an annular slot in the bottom end cap, even though actual waste extraction occurs through the scoop. If the slot is of width $\Delta\xi$ in scale heights at radial location ξ_w and gas exits with speed w_B, the waste flow rate from the centrifuge W is given by:

$$W = \rho_w e^{-\xi_w} \pi a^2 \Delta\xi \, w_B/A^2$$

The stream function Ψ_B is obtained from Eq. (43) with radial position expressed in scale height units, ρ_{eq} given by Eq. (11), and $w = - w_B$:

$$\Psi_B = - \frac{e^{\xi}}{2 A^2 \Omega a} \int_0^{\xi} e^{-\xi'} w_B \, d\xi' \qquad (46)$$

The integral in Eq. (46) is zero up to $\xi_w - \Delta\xi/2$, increases linearly up to $\xi_w + \Delta\xi/2$, and is constant thereafter.

To determine Ψ_∞ in Eq. (44), the right hand sides of Eqs. (A-11) and (C-8) are equated and the Master potential introduced by use of Eq. (A-13). For $r \simeq a$, this procedure yields:

$$\Psi_\infty = \frac{2 A^2 e^{\xi}}{\rho_w \Omega a^5} \left(\frac{\partial \chi}{\partial \xi}\right)_{\eta = 0} \qquad (47)$$

The quantity ϕ_B in Eq. (44) denotes the specified thermal and mechanical conditions on the bottom end cap (i.e. an end cap temperature ΔT_B larger than the bulk has, as shown in Fig. 3a, and/or a bottom disk with angular velocity $\Omega - \Delta\Omega_B$):

$$\phi_B = \frac{\Delta T_B}{T_o} + 2 \frac{\Delta\Omega_B}{\Omega} \qquad (48)$$

The first term on the left hand side of Eq. (44) represents the same parameter evaluated in the Stewartson layer at the bottom of the centrifuge. Integrating Eq. (27) along the bottom of the Stewartson layer gives:

$$\Phi_\infty \equiv \Phi(\xi,0) = \Phi(0,0) - \frac{2S}{\varepsilon A^2 \rho_w \Omega a^5} \int_0^\xi \left(\frac{\partial \chi}{\partial \eta}\right)_{\eta=0} d\xi' \qquad (49)$$

where ϕ (0, 0) is evaluated at the rotor wall at a distance equal to the Ekman layer thickness from the bottom end cap. If the temperature is discontinuous at the rotor corner (as in Fig. 3 a), then:

$$\Phi\ (0,\ 0) = 0 \qquad (50a)$$

For the temperature profile of Fig. 3 b, on the other hand,

$$\Phi\ (0,\ 0) = \Delta T_B/T_o \qquad (50b)$$

Eq (50a) corresponds to bottom end cap thermal drive, whereas Eq. (50b) represents pure wall thermal drive. In either case, the azimuthal velocity perturbation v is zero because ϕ is evaluated at the rotor wall, not on the bottom end cap, which may be rotating at an angular velocity different from that of the wall. Substituting Eqs. (46), (47), and (49) into Eq. (44) yields:

$$\Phi(0,0) - \Phi_B - \frac{2S}{\varepsilon A^2 \rho_w \Omega a^5} \int_0^\xi \left(\frac{\partial \chi}{\partial \eta}\right)_{\eta=0} d\xi'$$

$$= \frac{4 S^{3/4}}{\sqrt{\varepsilon}}\ e^{\xi/2} \left\{ \frac{2A^2}{\rho_w \Omega a^5} \left(\frac{\partial \chi}{\partial \xi}\right)_{\eta=0} + \frac{1}{2A^2 \Omega a} \int_0^\xi e^{-\xi'} w_B d\xi' \right\} \qquad (51)$$

In order to convert Eq. (51) (and the corresponding top end cap matching condition) to usable axial boundary conditions for the Master equation, χ is expressed as $\chi^E + \chi^0$. With χ^E given by Eq. (42), this substitution converts Eq. (51) into:

$$\sum_{n=1}^{\infty} P_n(\xi) D_n + \sum_{n=1}^{\infty} Q_n(\xi) E_n = R_B(\xi) \qquad (52)$$

where

$$P_n(\xi) = \frac{8 S^{3/4} A^2}{\sqrt{\varepsilon}\, \rho_w \Omega a^5} e^{\xi/2} \frac{df_n^E}{d\xi} - \frac{2S}{\varepsilon A^2 \rho_w \Omega a^5} \left(\frac{\lambda_n}{B}\right) \int_0^{\xi} f_n^E d\xi' \qquad (53a)$$

$$Q_n(\xi) = \left\{ \frac{8 S^{3/4} A^2}{\sqrt{\varepsilon}\, \rho_w \Omega a^5} e^{\xi/2} \frac{df^E}{d\xi} + \frac{2S}{\varepsilon A^2 \rho_w \Omega a^5} \left(\frac{\lambda_n}{B}\right) \int_0^{\xi} f_n^E d\xi' \right\} \exp\left(\frac{-\lambda_n}{B}\right) \qquad (53b)$$

and

$$R_B(\xi) = -\frac{4 S^{3/4}}{\sqrt{\varepsilon}} e^{\xi/2} \left\{ \frac{2A^2}{\rho_w \Omega a^5} \left(\frac{\partial \chi^0}{\partial \xi}\right)_{\eta=0} + \frac{1}{2A^2 \Omega a} \int_0^{\xi} e^{-\xi'} w_B \, d\xi' \right\}$$
$$- \frac{2S}{\varepsilon A^2 \rho_w \Omega a^5} \int_0^{\xi} \left(\frac{\partial \chi^0}{\partial \eta}\right)_{\eta=0} d\xi' + \phi(0,0) - \phi_B \qquad (54)$$

are known functions of the scale height variable ξ; the derivatives and integrals of the end mode eigenfunctions f_n^E are obtained by the same methods that produced the curves of Fig. 4. The corresponding operations on the zero eigenvalue mode χ^0 are performed with the aid of Eqs. (32) and (33), in which the constants are known.

The formula corresponding to Eq. (52) for the top end cap is:

$$\sum_{n=1}^{\infty} Q_n(\xi) D_n + \sum_{n=1}^{\infty} P_n(\xi) E_n = -R_T(\xi) \qquad (55)$$

where $R_T(\xi)$ differs from $R_B(\xi)$ of Eq. (54) by the appearance of a plus sign in front of the first term on the right hand side and by the use of the specified exit velocity through the top end cap, w_T, in place of $-w_B$. In addition, ϕ_B is replaced by ϕ_T, reflecting thermal conditions at the top end cap, and $\phi(0,0)$ in Eq. (54) becomes $\phi(0,1)$, which is equal either to zero or to $\Delta T_T/T_o$, the latter applying if the top end cap is cooled. Note that the end modes are active even when there are no end drives (i.e., $\phi(0,0) = \phi_B$); the end mode solutions enter even in the cases of wall thermal or feed drives.

If the summations in Eqs. (52) and (55) are terminated after N terms, 2N coefficients D_n and E_n need to be determined. This is accomplished by selecting N radial positions between $\xi = 0$ and $\xi = \xi_o$ and applying Eqs. (52) and (55) to each position. The resulting 2 N algebraic equations are then solved for the N values of D_n and the N values of E_n. Calculation of these coefficients completes the determination of all of the constants in the solution for the Master potential for the specified thermal, mechanical, and feed conditions of the centrifuge. Any of the physical characteristics of the flow can now be computed from the Master potential; in particular, the axial mass velocity needed for the separation analysis is given by Eq. (15).

B.6 Computed velocity profiles

As indicated by Eq. (1), the circulation developed by each of the driving modes can be computed individually and the resulting components of the axial velocity added together to produce the total countercurrent. In this section, we give illustrative examples of the calculated flow patterns for wall thermal drive and for scoop drive, which are the most important techniques for flow generation from a practical point of view.

Wall Thermal drive

The computed profiles of the axial mass velocity at two axial locations in the rotor are shown in Fig. 6 [after Wood and Morton [10]]. These circulatory flows are produced by an extremely small temperature gradient ; the temperature of the rotor wall is 1 K hotter at the bottom than at the top, for a rotor which is over 3 m long. This driving force produces maximum speeds of the gas descending near the wall of $\sim$ 4 cm/s. Because there is no feed in this example, the areas under the curves in the figure are zero. However, the strength of the countercurrent flow can be obtained by integrating the mass velocity from the axis ($\xi = \infty$) to the crossover point ($\xi = \xi_{co}$, which is where w changes sign) :

$$\text{strength of countercurrent} = \frac{\pi a^2}{A^2} \int_{\xi_{co}}^{\infty} \rho_{eq}\, w\, d\xi \qquad (56)$$

At the midplane ($\eta = 1/2$) the flow in the countercurrent is 30 - 40 mg UF_6/s. This value is of the same order of magnitude as the product or waste flow rates in a typical centrifuge . If the temperature difference between the top and bottom end caps were 10 K instead of 1 K, the maximum velocity and the strength of the countercurrent would be 10 times larger than the values obtained from Fig. 6. Thus, it is relatively easy to obtain reflux ratios (strength of countercurrent/ net upflow or downflow) in excess of ten, which renders any feed effect a small perturbation on the countercurrent established by the primary drive.

Figure 6 contains curves for two rotor speeds, 400 m/s and 700 m/s. The shapes of the velocity profiles in terms of the real radial position r are not much different for these two cases despite the separation seen in Fig. 6, which is due to use of the scale height unit. At 700 m/s, the countercurrent extends out to $\sim$ 6 scale heights, whereas at 400 m/s , it dies out by $\sim$ 2 scale heights from the wall. However, using Eq. (10) to convert scale heights to fractional radius, both of these figures correspond to a Stewartson layer contained within the outermost 10% of the rotor radius. Or, the Stewartson layer is $\sim$ 9 mm thick in the two cases. The velocity crossover points occur at a fractional radius of $\sim$ 0.98 for both rotor speeds. Note that the crossover point moves outward (in scale height units) as the rotor speed increases. In the limit of high speeds the radial shape of the profile appears to be approaching that deduced previously by several authors[6, 15, 18] by elementary analyses of the hydrodynamics :

$$\rho_{eq} \; w \propto e^{-\xi} - (1 + 2\xi)e^{-2\xi} = f_w(\xi) \qquad (57)$$

This solution also corresponds to the axial velocity obtained from the $f_1^0(\xi)$ zero eigenvalue solution given by Eq (33a) (i.e., the second derivative of f_1^0 has the same ξ -dependence as Eq (57),).

Although this particular aspect of the zero eigenvalue solution has nearly the correct radial shape, its axial behavior given in Eq (55) is very different from the correct one seen in Fig. 6. Thus, the end mode solution is essential to a correct analysis of the circulation eyen when

the countercurrent is not driven from the ends. For each of the two rotor speeds considered, Fig. 6 displays the profiles at two axial positions in the rotor. The profiles have roughly the same radial shape at all axial locations. The amplitudes are greatest at the midplane and decrease to zero towards either end in a symmetric manner. The countercurrent induced by a constant temperature gradient along the rotor wall can be expressed empirically by the formula :

$$(\rho_{eq}\, w)_w = B'_w f_w(\xi)\, h_w(\eta) \tag{58}$$

where B'_w is an amplitude factor which is proportional to the imposed wall temperature gradient, $f_w(\xi)$ is a radial shape function approximated by Eq (57) and $h_w(\eta)$ gives the axial variation of the strength of the countercurrent :

$$h_w(\eta) = \left[4\eta(1-\eta)\right]^c \tag{59}$$

where $c = 2/3$

Scoop drive

Scoop-driven internal flow calculation is more difficult than that for the wall-driven flow just discussed. In the theoretical formulation outlined here, as in other recent studies [5], the scoop is simulated by a bottom end cap rotating more slowly than the rotor wall. In reality, the scoop is a stationary object placed inside the high speed rotating gas, and a realistic simulation of its flow-driving capacity would probably treat it as an internal source of heat (due to friction) and a sink of momentum (due to drag) located in the gas near but not at the bottom of the rotor. The theory described here does not contain provision for internal sources or sinks of mass, momentum or energy, but the detailed development of the Onsager model by Wood and Morton [10] allows for such terms, which lead to a nonhomogeneous version of Eq. (9). Scoop simulation by a velocity defect of the bottom end cap leaves unanswered the question of how to relate the angular speed defect $\Delta\Omega_B$ to the size, shape, and radial placement of the scoop tip. As can be seen from Eq. (48), scoop drive simulation by an angular velocity deficit would produce exactly the same type of velocity profile in the rotor as would a heated bottom end cap, which does not seem intuitively reasonable given the physical difference between

the two means of inducing a countercurrent.

Nonetheless, to obtain some idea of the type of internal circulation to be expected from a bottom scoop, Fig. 7 reproduces the numerically computed profiles from the French code CENTAURE [19] for the same centrifuge to which the curves in Fig. 6 apply. For the scoop drive case, the angular velocity defect $\Delta \Omega_B / \Omega$ was chosen to produce the same circulation strength (as defined by Eq (56)) at $\eta = 0.05$ as is achieved by wall thermal drive at the rotor midplane. As depicted in Fig. 7, the radial variation of the axial mass velocity has roughly the same shape for scoop drive at $\eta = 0.05$ as does wall thermal drive at $\eta = 0.5$. However, instead of a symmetric amplitude decay towards both ends, scoop drive decreases monatonically from the bottom to the top. This is a result of the exponential decay of the end modes contained in Eq (42). Within a short distance from the scoop, the higher modes essentially vanish and only the pure exponential decay characteristics of the first end mode remains. Moreover, the radial shape of the flow induced by the scoop is not self-preserving, as it is for wall thermal drive. The crossover point moves towards the axis as height in the rotor increases. Despite these complications, the scoop-driven countercurrent will be approximated by a simple single-term product solution for use in the separation analysis of the following section:

$$(\rho_{eq} w)_s = B'_s f_s(\xi) h_s(\eta) \qquad (60)$$

where B'_S is a single adjustable amplitude factor for this driving mechanism. To very roughly model the some what broader radial distribution of the scoop-driven countercurrent than that due to wall thermal drive, $f_s(\xi)$ is taken to be of the same form as Eq (57) but an adjustable parameter b (< 1) is added :

$$f_s(\xi) = e^{-b\xi} - (1+2b\xi)e^{-2b\xi} \qquad (61)$$

Axial decay is approximated by :

$$h_s(\eta) = \exp(-\eta / \eta_s) \qquad (62)$$

where η_s is an axial decay length.

Feed drive

To represent the internal flow arising from feed injection at axial location η_F, we utilize the last term in Eq (32), with the constants B_2 and C_2 determined by the feed conditions. If the latter are expressed by Eqs (39) and (40), and Eq (15) is used to convert the second derivative of the Master potential to the axial mass velocity, we find :

$$(\rho_{eq} w)_F = \frac{2A^2}{\pi a^2} P \, e^{-\xi}(1 - e^{-\xi}) \qquad (63a)$$

in the enriching section of the centrifuge, and :

$$(\rho_{eq} w)_F = -\frac{2A^2}{\pi a^2} W \, e^{-\xi}(1 - e^{-\xi}) \qquad (63b)$$

in the stripping section.

Just as in the case of wall thermal drive, these solutions are only rough approximations because the end mode contributions introduced by application of the axial boundary conditions of Eq (52) and (55), wherein the zero eigenvalue solutions enter via the factor R_B of Eq (54) and the corresponding factor R_T for the top, have not been taken into account. In addition, the effects of feed spread (i.e. the distribution of the input gas over a significant axial interval), the angle of feed injection, and the angular momentum deficit of the feed gas are lost by this simple treatment. However, because feed affects the total countercurrent by only about 10% in a practical machine, the approximations given by Eqs. (63a) and (63b) should be adequate for the separation calculations of the following section.

C. SEPARATION THEORY

C.1. The diffusion-convection equation and its boundary conditions

The object of separation analysis of the gas centrifuge is to

determine the product and waste concentrations for specified feed concentration, throughput, cut and internal gas velocities. The equation to be solved is :

$$\rho u \frac{\partial x}{\partial r} + \rho w \frac{\partial x}{\partial z} = \frac{\rho D}{r} \frac{\partial}{\partial r}\left[r \frac{\partial x}{\partial r} + \frac{\Delta M}{RT_o} (r\Omega+v)^2 x(1-x) \right] + \rho D \frac{\partial^2 x}{\partial z^2} \qquad (64)$$

where the perturbation velocity components, u, v, w are obtained from the hydrodynamic analysis outlined in section B and x the isotopic fraction of the U-235. The density-self diffusion coefficient product, ρD, is a constant equal to 2.3×10^{-4} g UF_6/cm-sec at 300 K. Two terms in Eq. (64) may be eliminated at the outset.

The first term on the left hand side represents radial convection of U-235. It appears when the axial mass velocity varies with height in the rotor because when this is so, overall mass conservation, Eq.(7a), requires that ρu be nonzero. However, because of the large length-to-radius ratio of the rotor, even sizeable axial variation of ρw does not generate radial mass velocities sufficiently large to render radial convection important. Consequently, this term in Eq. (64) is deleted.

The appearance of the azimuthal perturbation velocity v on the right hand side of Eq. (64) arises from the fact that the pressure diffusion phenomenon depends upon the local tangential velocity, not on the wheel flow velocity. However, v is everywhere much smaller than $r\Omega$, and can also be neglected.

With the above omissions and with the approximation $\rho w \simeq \rho_{eq} w$, Eq. (64) becomes :

$$\rho_{eq} w \frac{\partial x}{\partial z} = \frac{(\rho D)}{r} \frac{\partial}{\partial r}\left[r \frac{\partial x}{\partial r} + \frac{\Delta M \Omega^2}{RT_o} r^2 x(1-x) \right] + (\rho D) \frac{\partial^2 x}{\partial z^2} \qquad (65)$$

The outer radial boundary conditions for Eq. (65) is:

$$\left[\frac{\partial x}{\partial r} + \frac{\Delta M \Omega^2}{RT_o} rx(1-x) \right]_{r=a} = 0 \qquad (66)$$

Equation (66) prohibits transport of matter through the rotor wall. For the purpose of solving the diffusion-convection equation, the imaginary inner boundary at $r = r_o$ [or ξ_o of Eq. (23)] may be regarded as a solid wall rotating at the wheel flow velocity. Except in the zone of feed injection, the strong centrifugal force prevents significant radial mass transport at the inner edge of the Stewartson layer, or:

$$\left[\frac{\partial x}{\partial r} + \frac{\Delta M \Omega^2}{RT_o} rx(1-x)\right]_{r=r_o} = 0 \qquad (67)$$

However, if the axial zone over which feed injection occurs is small compared to the rotor length, feed injection can be considered to occur at a unique axial location z_F. In this case, the feed effects appear in the axial boundary conditions.

The axial boundary conditions for Eq. (65) are:

$$\left(\frac{\partial x}{\partial z}\right)_{z=0} = 0 \qquad (68)$$

and

$$\left(\frac{\partial x}{\partial z}\right)_{z=Z} = 0 \qquad (69)$$

When applied to the solid part of an end cap this condition represents zero mass flux of U-235. However Eqs. (68) and (69) are also used at the radial locations of the ports for gas extraction on the end caps. In this case, they imply that the exit flux is primarily due to convection with a negligible portion due to molecular diffusion.

After solution of the diffusion-convection equation, the product and waste compositions are calculated from:

$$x_p = \frac{2\pi}{P} \int_{r_p - \Delta_p}^{r_p + \Delta_p} \rho_{eq} w(r, Z) x(r, Z)\, r\, dr \qquad (70a)$$

and

$$x_w = -\frac{2\pi}{W} \int_{r_w - \Delta_w}^{r_w + \Delta_w} \rho_{eq} w(r, 0) x(r, 0)\, r\, dr \qquad (70b)$$

The product removal port is modeled as an annulus of radius r_p and width $2\Delta_p$, and the waste removal port is treated in a similar fashion. The negative sign is attached to the right handside of Eq (70b) because the axial velocity component w leaving the bottom end cap is negative in the rotor coordinate system. The unknown exit compositions x_p and x_w are related by the overall U-235 balance on the centrifuge :

$$x_F L = x_p P + x_w W \qquad (71)$$

Nakayama and Torii [20], Kai [21] and Soubbaramayer [5] have solved the diffusion equation numerically using boundary conditions equivalent to those outlined above.

C.2. The Onsager-Cohen solution

In his book, Cohen presents a solution of the diffusion-convection equation in a countercurrent gas centrifuge [1]. The technique employed by Cohen is closely related to the method developed by Furry, Jones and Onsager [22] for analyzing isotope separation in the thermal diffusion column, so the modification for the gas centrifuge is aptly termed the Onsager-Cohen solution method. This method consists of replacing direct solution of Eq (65) by the simpler problem of solving its radially integrated form, which is [6] :

$$\begin{pmatrix} x_p P \\ -x_w W \end{pmatrix} = -2\pi(\rho D) \int_0^a r\left(\frac{\partial x}{\partial z}\right) dr + 2\pi \int_0^a \rho_{eq} wxr dr \qquad (72)$$

On the left hand side, of this equation, $x_p P$ applies to the enriching section (above the feed injection point) and $-x_w W$ is used in the stripping section. The approximations in the Onsager-Cohen solution method include :

1. Replacing radial integrals over the concentrations by a common "average" value.

2. Dropping the axial diffusion term in Eq. (65).

In solving the diffusion-convection equation using the Onsager-Cohen method careful attention must be paid to the approximations inherent in the analysis. In Appendix D it is shown that four different radial averages are implicit in the Onsager-Cohen solution method. All but one are essentially equal to that obtained by using a weighting function given by the density distribution of Eq. (11) in the radial average. If all of these radial averages are assumed to be identical, the axial enrichment equation for the radially-averaged concentration x is given by:

$$\frac{dx}{d\eta} = g_p(\eta) \left[x(1-x) - \gamma_p(\eta) P (x_p - x) \right] \tag{73}$$

where:

$$g_p(\eta) = \frac{2\left(\frac{\Delta M}{M}\right)\left(\frac{Z}{a}\right)\int_0^{A^2}\left[F(\xi,\eta) - Pe^{-\xi}\right] d\xi}{\mathcal{D} + \frac{1}{\mathcal{D}A^2}\int_0^{A^2}\frac{\left[F(\xi,\eta) - Pe^{-\xi}\right]\left[F(\xi,\eta) - P(1-\xi/A^2)\right]}{1-\xi/A^2} d\xi} \tag{74}$$

and

$$\mathcal{D} = 2\,\pi\, a\, \rho\, D \tag{75}$$

is a diffusive transport parameter with the units of flow rate. The coefficient γ_p is :

$$\gamma_p(\eta) = \left\{ \left(\frac{\Delta M}{M}\right) \int_0^{A^2}\left[F(\xi,\eta) - Pe^{-\xi}\right] d\xi \right\}^{-1} \tag{76}$$

$F(\xi, \eta)$ is the flow function defined by Eq (2).

Equation (73) applies to the enriching section of the centrifuge ($n_F \leq \eta \leq 1$). A similar equation can be derived for the stripping section:

$$\frac{dx}{d\eta} = g_w(\eta) \left[x(1-x) - \gamma_w(\eta) W (x - x_w) \right] \tag{77}$$

The coefficients g_w and γ_w are of the same form as Eqs (74) and (76) except that P is replaced by -W.

The differences between the axial enrichment equation of the early Onsager-Cohen method (Eqs. (52) and (59) of Ref. 6) and those derived here are :

1. Axial variation of the flow-dependent coefficients is included.
2. The coefficients g and γ are different in the enricher and stripper sections for the following reasons :

   a) The inclusion of the axial diffusion term in the derivation of Eq (74) supplies the term $P(1 - \xi/A^2)$ in the denominator and a term $-W(1 - \xi/A^2)$ in the comparable stripper coefficient.

   b) Proper treatment of the wall concentration in the derivation of Eq (73) introduces the $Pe^{-\xi}$ terms in g_p and γ_p and $-We^{-\xi}$ terms in g_w and γ_w.

   c) The product and waste flow rates affect the flow function F through the F_F component in Eq (3). F_F is proportional to P in the enricher and to -W in the stripper.

Solution method

Equations (73) and (77) cannot be solved analytically if the coefficients g and γ are axially dependent*. However, the following numerical scheme converges rapidly :

---

* Actually, formal analytical solution is possible when $x << 1$ but the double integrals appearing in the solution must be evaluated numerically [5].

1. The feed concentration x_F, the cut $\theta = P/L$ and the throughput $L = P + W$ are specified, as are the rotor geometry (a and Z) and the speed (Ω or A^2).

2. The hydrodynamic analysis of section B provides the axial mass velocities for each flow mode. This may require specification of the Ekman number (ε). The mass velocities are converted into flow functions and added together according to Eq (3). The flow coefficients g_p, g_w, γ_p and γ_w are calculated according to Eqs (74) and (76) and the corresponding stripper formulas.

3. A value of x_p is guessed. The best first guess is obtained by using the axially averaged values of g and γ in the analytic solution of the separation problem given in Ref. 6.

4. The value of x_w corresponding to the assumed x_p is determined from the overall material balance of Eq. (71).

5. Eq (77) is integrated numerically from $\eta = 0$ until the specified feed injection position, η_F, is reached. Alternatively if the condition of no-mixing is imposed instead of specification of the feed point, the integration of the stripper equation is carried up to the axial position at which $x = x_F$.

6. In the enriching section integration is continued using Eq (73) until the top of the centrifuge ($\eta = 1$) is attained.

7. The composition calculated in step 6 is compared to the guess in step 3. If these two do not agree satisfactorily, the initial guess is improved (by Newton's rule, for example) and the calculation repeated.

8. If the guessed and calculated product compositions are in satisfactory agreement the separative power can be computed by :

$$\delta U = 21.2\, L \left[\theta V(x_p) + (1 - \theta) V(x_w) - V(x_F) \right] \qquad (78)$$

where V(x) is the value function defined by

$$V(x) = (2x - 1)\ln[x/(1 - x)] \qquad (79)$$

The numerical factor in Eq (78) provides δU in kg U/year from throughput L with units of mg UF_6/sec.

C.3. The performance function

The separative power of a centrifuge of given geometry (rotor height and radius) and specified peripheral speed (the highest that the materials of construction can withstand) depends upon the internal variables controlling the component drives and upon the operating variables, which are the cut θ and the throughput L. These last two parameters appear explicitly in the separation theory and indirectly via the feed drive component of the flow function. In general terms the separative power of a centrifuge may be expressed in the functional form :

$$\delta U\ (L,\ \theta\ ,\ \text{internal variables})$$

where the term "internal variables" includes all of the adjustable parameters controlling the various drives. The centrifuge performs most efficiently when the internal variables are adjusted (at each combination of L and θ) so that the separative power is a maximum. The optimized separative power is therefore a function only of the operating variables L and θ . Using an asterisk to denote optimization with respect to all internal variables, the function δU^* (L, θ) is called the performance function of the centrifuge. Provided all the internal variables have been considered in the optimization process, the isotope separating capability of the centrifuge is completely defined by its performance function. Assuming that the rotor geometry and the speed are fixed, each point on the performance function (i.e., at each L and θ) requires optimization of δU with respect to the following internal variables:

1. the wall temperature gradient (or more generally the temperature distribution along the rotor wall).

2. the temperature difference between the end caps and the bulk gas at the ends of the rotor.

3,4. Two variables controlling scoop drive (e.g. radial location of the scoop tip and the size of the tip, or, for analytical flow modeling, the angular velocity difference between a hypothetical bottom disk and the rotor wall and the radius of the bottom disk).

5. The gas density at the rotor wall.

6. The axial feed injection location

This list of six controllable variables probably represents the minimum number which have to be considered in flow optimization. Because of the large number of variables involved, determination of the performance function either analytically or experimentally is a costly procedure. One way of greatly speeding up the hydrodynamic calculation is to exploit the superposition property of the flow drives [Eq (3)]. Each of the component flow functions depends upon only one or two of the six variables controlling the total flow field. In addition, each of the component flow functions is proportional to the externally applied driving force for the particular mode, so that Eq (3) can be further decomposed into :

$$F = q' F'_w + \phi_T F'_e + \phi_B F'_s + \begin{pmatrix} P \\ -W \end{pmatrix} F'_F \qquad (80)$$

where q' is the dimensionless temperature gradient along the rotor wall [Eq (37)] and ϕ_B is the parameter which is responsible for the countercurrent induced by the bottom end cap temperature difference and by the scoop [(Eq (48)] . ϕ_T is the corresponding parameter which accounts for active cooling (if any) of the top end cap.

The modified flow functions F'_w and F'_e depend upon the dimensionless position variables ξ and η and are parametric in the gas density at the wall (or the Ekman number). A library of these flow functions can be prepared from the detailed hydrodynamic codes for several values of ρ_w in the range of practical importance and the flow functions for arbitrary ρ_w reconstructed by interpolation from the library cases.

The modified scoop flow function F'_s is parametric in the gas density at the wall and in the second variable controlling scoop drive, and a two dimensional array of F'_s profiles would be needed for the library. There remains the problem of how to relate the physical features of the scoop (size, shape and location) to the angular velocity defect $\Delta\Omega_B$ utilized in the theory, or, for that matter, whether the concept of an angular velocity defect is a suitable means of modeling the complex scoop-gas interaction. This problem has not been broached in the open literature.

The feed drive component in Eq (80) has been assumed to be proportional to the net upflow in each section of the rotor (P in the enricher and -W in the stripper). The modified feed drive flow function F'_F depends upon gas density at the wall and on feed injection location.

In order to develop the concept of the performance function without the difficulty associated with detailed hydrodynamic calculations, we utilize the simplified flow functions presented in Section B.6 and consider a centrifuge with internal gas circulation produced by a combination of feed, scoop and wall thermal drives. In this illustrative optimization calculation, b in Eq (61) is assumed to be 1/2 for scoop drive and unity for wall thermal drive. In addition, c in Eq (59) is assigned the value of 2/3 and η_s in Eq (62) is taken as 0.5. The flow function is :

$$F(\xi,\eta) = B_w\left[e^{-\xi} - (1+\xi)e^{-2\xi}\right]\left[4\eta(1-\eta)\right]^{2/3} + B_s\left[e^{-\xi/2} - (1+\xi/2)e^{-\xi}\right]e^{-2\eta} + \begin{pmatrix} P \\ -W \end{pmatrix}\left[2e^{-\xi} - e^{-2\xi}\right] \tag{81}$$

Eq. (81) satisfies the integral constraints :

$$F(0,\eta) = \begin{cases} P \text{ in the enricher} \\ -W \text{ in the stripper} \end{cases}$$

The coefficients B_w and B_s include the parameters q' and ϕ_B appropriate to these two driving modes. These coefficients are regarded as adjustable parameters which are to be determined by the optimization procedure.

Typical values of the fixed parameters A^2, $\mathcal{D}$, and Z/a were selected and δU determined as a function of B_w and B_s for L = 100 mg UF_6/sec and $\theta = 0.4$. The Onsager-Cohen solution method described in Sec. C.2., in conjunction with the condition of no-mixing at the feed injection point, was employed in solving the diffusion equation.The results are shown in the topographical plot of Fig. 8, where the curves represent contours of constant separative power. The centrifuge performs most efficiently with a mixture of scoop and wall thermal drive indicated by the peak located at the cross in the plot. This optimum is larger than can be achieved if the centrifuge is driven either by the scoop alone or by a wall temperature gradient alone.

The reflux ratio is defined as the magnitude of the circulatory flow divided by the net flow. The former is equal to the non-feed portion of the flow function at the location of the change in sign of $\rho_{eq} w$. The latter is the product flow rate in the enricher or the waste flow rate in the stripper. For the example using Eq (81) which results in the plot of Fig. 8, the reflux ratio is 12 at the waste end and 2.6 at the product end. At the feed point, the reflux ratio is 15 on the enricher side and 10 on the stripper side.

The axial concentration distribution for conditions at the peak is shown in Fig. 9. Most of the enrichment occurs in the upper part of the centrifuge, for the following reason. The decrease in the flow function towards the top causes a larger reduction in the integral in the denominator of Eq (74) than it does in the integral in the numerator. Hence, g_p increases near the top and by Eq (73) the concentration gradient steepens. Figure 9 also shows that the feed point for no-mixing occurs at an axial location well above the expected value for axially invariant flows in the close separation limit, for which $\eta_F = \theta$ (Ref. 6).

The contours in Fig. 8 were computed with the restriction of no-mixing at the feed injection point. As in the ideal cascade, it is usually assumed that the highest separative power in a single centrifuge is attained by adhering to this rule. However, Fig. 10 shows that this criterion for feed injection need not result in the best machine performance. In the example treated here, the maximum separative power occurs when the relative feed injection height is 0.51 rather than the no-mixing condition of 0.59. There is a significant penalty for introducing the feed at an off-optimum axial position.

The peak marked by the cross in Fig 8 represents one point on the performance function of a centrifuge with internal circulation induced by scoop, feed and wall thermal drives. To illustrate entire performance functions for various types of internal drives with only a single adjustable parameter to consider, flow optimization calculations have been performed separately for scoop plus feed drive and for wall thermal plus feed drive. The radial shape of the non-feed component is given by Eq (61) and the axial shape by either Eq (59) or Eq (62) As in the previous example, the feed is represented by an axially invariant flow function with the radial shape of Eq (63) . The optimization is performed on the single magnitude parameter B for the internal drive considered. Throughputs range from 25 to 100 mg UF_6/sec and cuts from 0.2 to 0.8 are considered.

Figure 11 shows the performance function for axially invariant flow ($c = 0$ in Eq (59) and with $b = 1$ in the radial shape profile. The optimized separative power δU^* is relatively insensitive to cut and increases slightly with throughput. Fig. 12 shows the effects of changing the radial shape and using $c = 2/3$ in the axial velocity profile of Eq (59) The performance function for $b = \frac{1}{2}$ is nearly twice as great as it is for $b = 1$. This effect is best understood in terms of the flow pattern efficiency e_F introduced by Cohen[1] and defined by Eq. (63) of Ref.23. In terms of the scale height variable, e_F with no feed is given by

$$c_F = \frac{2}{A^2} \frac{\left\{\int_0^{A^2} F d\xi\right\}^2}{\int_0^{A^2} \frac{F^2 d\xi}{1-\xi/A^2}} \qquad (82)$$

The flow pattern efficiency is unity when the flow function is proportional to r^2, or $F \propto 1 - \xi/A^2$. However, using the radial shape given by Eq (61) in Eq (82), we find that E is proportional to 1/b, which qualitatively agrees with the difference between the performance functions shown in Fig. 12 for $b = \frac{1}{2}$ and $b = 1$. As a general rule, those radial shapes which extend furthest into the inner core of the rotor give the best performance.

The effect of the axial shape of the flow function can be seen by comparing the performance functions for the axially invariant flow shown in Fig. 11 with the lower performance function surface in Fig. 12. These two performance functions differ only in the prescribed axial shape of the flow function used to compute them, the latter represented by Eq. (59) with $c = 2/3$ and the former a constant. The axially tapered flow function yields $\sim$ 19% higher separative power at a cut of ½ than is obtainable from the axially invariant flow. According to May [24], this improvement is due to attainment of an ideality efficiency of nearly 100%. A centrifuge with nondecaying internal circulation is analogous to a square cascade, for which the maximum ideality efficiency is 81% [23]. If the flow in the interior of the centrifuge is tapered to resemble that of an ideal cascade rather than that of a square cascade, the ideality efficiency increases to 100%. In order to prove this proposition for flow functions derived from simple hydrodynamics of the type $F(\eta, \xi) = Bh(\eta)f(\xi)$, we rewrite Eq. (73) in the form:

$$\frac{dx}{d\eta} = 2\left(\frac{Z}{a}\right)\mathcal{D}\ \frac{C_1 x(1-x)H - P\,(x_p - x)}{\mathcal{D}^2 + C_2 H^2} \tag{83}$$

where $H(\eta) = Bh(\eta)$ and C_1 and C_2 are:

$$C_1 = \frac{\Delta M}{M}\int_0^{A^2} f(\xi)\,d\xi$$

$$C_2 = \frac{1}{A^2}\int_0^{A^2} \frac{f^2(\xi)\,d\xi}{1-\xi/A^2}$$

The terms involving P in these integrals have been neglected because they are much smaller than F. To determine the optimal axial shape of the circulation, we require that the axial concentration gradient be a maximum at all concentrations, which yields:

$$\frac{d}{dH}\left(\frac{dx}{d\eta}\right) = 0$$

Substituting Eq. (83) into the above formula gives the optimum value of H as a solution of the quadratic equation:

$$C_2 H_{opt}^2 - \frac{2C_2 P(x_p - x)}{C_1 x(1 - x)} H_{opt} - \mathfrak{D}^2 = 0 \qquad (84)$$

If we note that the group $C_2 H^2/\mathfrak{D}^2$ is the parameter m^2 of the Cohen theory (Eq. (97) of Ref. 6), the above equation is identical to the condition derived by Von Halle[25]. To determine the axial concentration distribution at these optimum conditions, Eq. (84) must be solved for H_{opt} as a function of x, substituted into the right hand side of Eq. (83), and the equation integrated numerically. Von Halle[25] has treated this problem in detail.

Except near the top of the centrifuge, the $\mathfrak{D}^2$ term in Eq. (84) is negligible, and the optimum axial shape of the internal flow can be expressed by:

$$\frac{H_{opt}}{P} = \frac{2(x_p - x)}{C_1 x(1-x)} \qquad (85)$$

or the optimum flow magnitude depends on composition in exactly the same way that it does for the ideal cascade. Eq. (85) shows that the flow function should be tapered so that it is a maximum at the feed point and decreases towards the top and bottom of the centrifuge (a formula for H_{opt} similar to Eq. (85) applies to the stripping section). If the feed is introduced into the center of the centrifuge, the axial shape represented by Eq. (85) is very close to that given by Eq. (59) with $c \simeq 2/3$. We have seen that changing the axial shape function from the

constant represented by the c = 0 in Eq. (59) to c = 2/3 form increases the performance function by ∿ 19%. If the axial flow shape is tapered even more strongly by using c = 1 in Eq. (59), the performance function decreases by ∿ 6% from the c = 2/3 surface of Fig. 12. Thus, an optimum axial shape for the circulatory flow in a gas centrifuge exists, and it is approximately that given by wall thermal drive for which c = 2/3 in Eq. (59). It should be recognized that these optimal axial shape analyses are valid only for flow functions which can be expressed as a product of a function of η and a function of ξ.

The existence of well-defined radial and axial flow function shapes for optimum separative performance provides a qualitative explanation for the location of the peak in the mixed scoop/wall thermal drive case of Fig. 8. The flow function for wall thermal drive has a nearly ideal axial shape, but compared to scoop drive, exhibits a radial profile which is too close to the rotor wall to give high efficiency. The flow function for scoop drive, on the other hand, has a poorer axial shape but a better radial pattern than the wall thermal drive flow function. The mixture of two parts of scoop drive and one part wall thermal drive best exploits the desirable features of each driving mode.

Figure 13 shows the performance function for a flow whose magnitude decays axially from the bottom end (typical of scoop drive). Contrary to the performance functions for axially symmetric flow shapes shown in Figs. 11 and 12, the best performance from bottom end-driven centrifuge is obtained at low cuts. This phenomenom is of importance in cascade design, and will be considered in the following section.

The dashed lines for the minimum and maximum throughputs in Figs. 12 and 13 show the effect of the correction factors involving P in the flow coefficients of Eqs. (74) and (76) (and W in the analogous coefficients applicable below the feed point) and of including the feed component in the total flow function. The dashed curves were computed by setting $F_F = 0$ in Eq. (3) and P = 0 in Eqs. (74) and (76) (and by letting W = 0 in the corresponding stripper coefficients). The results of ignoring feed

effects in the hydrodynamics and in the flow coefficients g and γ is to increase the predicted separative power by a few percent. At least from the idealized hydrodynamic model upon which the performance functions are based, the improvement over the original Onsager-Cohen model is slight.

The performance functions displayed in Figs. 11 - 13, which were computed from the idealized hydrodynamics represented by Eqs. (58 - 63). all show increasing separative performance as the throughput is increased. Whether this behaviour is an artifact of the particular velocity profiles utilized is not known. If the feed drive component of the flow function were properly modeled, the performance function might exhibit an optimum throughput as well as an optimum cut.

Fig. 12 shows that an optimum cut is predicted from pure wall thermal drive, while the scoop drive performance function of Fig. 13 increases monotonically with decreasing cut. The entire performance function for the dual drive case treated earlier was not computed, although it would likely turn out to be a blend of the lower performance function in Fig. 12 and the one in Fig. 13 and exhibit an optimum cut of less than 1/2. A three dimensional representation of the analytical or experimental procedure needed to establish the performance function $\delta U^*(L, \theta)$ for a centrifuge with two controllable internal flow parameters is shown in Fig. 14. The bottom surface represents the variation of separative power as the two driving mode strengths are varied for a single cut-throughput combination (in contour representation, this shape is depicted in Fig. 8). The peak P' of the lower surface becomes a single point P on the performance function sketched in the upper portion of Fig. 14. If the peak-search procedure represented by the lower sketch is repeated for all $L-\theta$ combinations, the entire performance function shown in the top of the figure is determined. For a real centrifuge, this process involves at least six rather than only two internal flow variables. Soubbaramayer and Billet[26] have studied internal flow optimization at fixed cut and throughput.

If the performance function posesses both an optimum cut and an optimum throughput, its representation would look very much like that shown in Fig. 14. The peak in such a performance function would then fix completely the best set of conditions at which tooperate the centrifuge. Barring mecha-

nical problems, there is little difficulty in operating at the optimum throughput. However, it will not in general be possible to operate the centrifuge as a unit in an ideal cascade at the optimum cut. The no-mixing requirement of the cascade dictates a definite relation between cut and separation factor, and this condition may force operation of the centrifuge in the cascade at an off-optimum cut.

D. IDEAL CASCADES FOR GAS CENTRIFUGES

D.1 Symmetric

In a conventional cascade, the heads and tails streams from a particular stage are sent to immediately adjacent stages (Fig. 15a). For this type of cascade to be ideal, the no-mixing condition

$$x_{p,i-1} = x_{w,i+1} \tag{86}$$

must be satisfied. Because the separating units which comprise each stage are operated in identical fashion, the heads and tails separation factors are independent of stage, which in the case of low enrichment, is expressed by:

$$\alpha = \frac{x_{p,\,i+1}}{x_{p,i}} = \text{constant with } i \tag{87a}$$

for the heads separation factor, and :

$$\beta = \frac{x_{w,\,i+1}}{x_{w,\,i}} = \text{constant with } i \tag{87b}$$

for the tails separation factor. The total separation factor is $\alpha\beta$. Substituting Eq (86) into Eq (87a) and comparing the result with Eq (87b) results in the symmetry condition :

$$\alpha = \beta \tag{88}$$

The U-235 balance on each stage is equivalent to the single centrifuge balance given by Eq (71). In terms of the heads and tails separation factors and the cut and the throughput, this equation is :

$$1 = \alpha\,\theta + (1 - \theta) / \beta \tag{89}$$

Taking Eq (88) into account, Eq (89) fixes a relationship between the separation factors and the cut :

$$\alpha = \beta = \frac{1 - \theta}{\theta} \tag{90a}$$

or

$$\theta = \frac{1}{\alpha + 1} = \frac{1}{\beta + 1} \tag{90b}$$

Thus, the larger the separation factor of the units, the lower the cut required for their operation in an ideal cascade. This condition in effect eliminates the cut as an independent variable if the units are to be operated in an ideal cascade. Instead of expressing the cut requirement in terms of the separation factors, it is more useful to work with the equivalent condition in terms of the separative power. For low enrichment, the value function of Eq (79) is approximately -lnx, and Eq (78) becomes :

$$\delta U = 21.2\ L \left[- \theta \ell n \alpha + (1 - \theta) \ell n \beta \right] \tag{91}$$

For the symmetric ideal cascade, α and β can be eliminated from this equation by Eq (90a) yielding :

$$\delta U = 21.2\ L\ (1 - 2\theta)\ \ln\left(\frac{1 - \theta}{\theta}\right) \tag{92}$$

This formula defines a surface of δU in (L, θ) space. This surface intersects the performance function $\delta U^{*}(L, \theta)$ along a space curve which is the locus of allowable operating points L and θ for the internally optimized separating units. If the throughput is selected, both the cut and the separating power are determined. One would want to select operating conditions along this space curve which produce the largest separative power for the following reason. To a good approximation, the cost of a centrifuge enrichment plant is proportional to the number of centrifuges in it. For a specified cascade separative capacity ΔU, the number of centrifuges needed is $\Delta U/\delta U$, which is minimized by making δU as large as possible.

Uranium enrichment by the gaseous diffusion method posesses two features which render it suitable for use in a symmetric cascade. First

the separation factor is very close to unity, so that the cascade cut required by Eq (90b) is very close to $\frac{1}{2}$. Second, the separative power of the gaseous diffusion barrier is relatively insensitive to cut. With centrifuges as separating units, however, neither of these conditions apply ; the separation factors are considerably larger than unity, and the separative power is a strong function of cut. As a result, other types of cascades (still ideal, or no-mixing) can provide more separative power than a symmetric cascade with the same number of centrifuges.

D.2. Asymmetric

Asymmetric cascades are designed to exploit the particular features of the cut-dependence of the separative power of gas centrifuges. The most important of these are bypass cascades, in which the heads and/or tails streams are delivered to units which are two or more stages away rather than to units in adjacent stages. The simplest variant of this type of asymmetry is the two-up, one-down cascade shown in Fig. 15b[4]. The no-mixing condition for this type of ideal cascade is:

$$x_{p,\ i-1} = x_{w,\ i+2} \tag{93}$$

and the heads and tails separation factors are :

$$\alpha = \frac{x_{p,\ i+1}}{x_{p,\ i-1}} = \frac{x_{p,\ i+1}}{x_{p,i}} \quad \frac{x_{p,i}}{x_{p,\ i-1}} = \text{constant with } i \tag{94a}$$

and

$$\beta = \frac{x_{w,\ i+1}}{x_{w,i}} = \text{constant with } i \tag{94b}$$

Using Eq (93) in Eq (94a) and taking Eq (94b) into account yields :

$$\alpha = \beta^2 \tag{95}$$

which is the asymmetry condition for the two-up, one-down ideal cascade. The cut-separation factor relationship for this cascade is obtained by using Eq (95) in the U-235 material balance given by Eq (89) , which results in :

$$\theta = \frac{\beta - 1}{\beta^3 - 1} = \frac{1}{\beta^2 + \beta + 1}$$

Replacing α in Eq (91) by β^2 and expressing β in terms of θ by Eq (96) yields the cascade condition in terms of the separative power :

$$\delta U = 21.2L\ (1 - 3\ \theta\ )\ \ln\left\{\sqrt{\frac{1}{4} + \frac{1-\theta}{\theta}} - \frac{1}{2}\right\} \qquad (97)$$

The advantage of a bypass cascade is illustrated for the scoop-driven centrifuge represented by the performance function in Fig. 13, where Eqs (92) and (97) are plotted for L = 100 mg UF_6/sec. The intersections of these lines with the upper solid curve of the performance function fix the cuts at which this type of centrifuge must be operated in the two types of ideal cascades. In the symmetric cascade, the required cut is 0.452 and the separative power is 38.5 SWU/Yr. In the two-up, one-down cascade, the centrifuge must be operated at a cut of 0.287 but the separative power is 42.2 SWU/Yr. This 10% improvement in performance is well worth the slightly more complex cascade piping required in the symmetric modification. Moreover, the two-up, one-down cascade provides two enriched streams, which may be desirable in blending products to customer specifications without incurring excessive separative work losses.

ACKNOWLEDGEMENT

The author would like to thank P. PLURIEN and SOUBBARAMAYER of the CEA for their generous assistance in many phases of preparing the manuscript. This work was supported by the Director, Office of Energy Research, Office of Basic Energy Sciences, Materials Sciences Division of the U.S. Department of Energy under Contract Number W-7405-ENG-48.

REFERENCES

1. Cohen, K.P., (1951) "The Theory of Isotope Separation as Applied to Large Scale Production of U^{235}". McGraw-Hill, New York.
2. Avery, D.G. and Davies, E. (1973) "Uranium Enrichment by Gas Centrifuge" Mills and Boon Ltd., London.
3. Villani, S., (1976) "Isotope Separation", Amer. Nucl. Soc.
4. Benedict, M., Pigford, T.H. and Levi, H.W. (1981) "Nuclear Chemical Engineering", Second Ed., McGraw-Hill, New York.
5. Soubbaramayer, (1979) in "Uranium Enrichment", S. Villani, Ed., Springer-Verlag.
6. Olander, D.R. (1972) "Technical Basis of the Gas Centrifuge", Adv. in Nucl. Sci. and Technol., 6, 105.
7. Olander, D.R., (1978) "The Gas Centrifuge", Scientific American, 239, no. 2, 37.
8. Stewartson, K. (1957) "On Almost Rigid Rotations", J. Fluid Mech., 3, 17.
9. Onsager, L., (1965) "Approximate Solutions of the Linearized Flow Equations". Unpublished report.
10. Wood, H.G. and Morton, J.B., (1980) "Onsager's Pancake Approximation for the Fluid Dynamics of a Gas Centrifuge", J. Fluid Mech., 101, 1.
11. Parker, H.M. and Mayo, T.T., (1963) "Countercurrent Flow in a Semi-infinite Gas Centrifuge", USAEC report UVA-279-63 U.
12. Ging, J. (1962) "Countercurrent Flow in a Semi-Infinite Gas Centrifuge in the Limit of High Angular Speeds", USAEC Report UVA-198-62 S.
13. Jacques, R., (1972) "Etude théorique du Contrecourant dans une Ultracentrifugeuse", CEA Report R-4336.
14. Brouwers, J.J.H., (1978) "On Compressible Flow in a Gas Centrifuge and its Effect on the Maximum Separative Power", Nucl. Technol., 39, 311.
15. Parker, H.M., (1973) "The With-Feed Pancake Model of the Internal Flow in a Gas Centrifuge". Unpublished report.
16. Morton, J.B., (1972) "Numerical Solution of the Eigenvalue Problem Associated with End-Driven Flows in Gas Centrifuges". Unpublished report.

17. Carrier, G.F. and Maslen, S.H., (1962) "Flow Phenomena in Rapidly Rotating Systems", USAEC Report TID 18065.

18. Lotz, M., (1973) "Die rien axiale Stromung in einer Gegenstrom-Gasultrazentrifuge", Atomkernenergie, 22, 41.

19. Lahargue, J.P. and Soubbaramayer, (1978) "A Numerical Model for the Investigation of the Flow and Isotope Concentration Field in an Ultracentrifuge", Comput. Method. Appl. Mech. and Eng., 15, 259.

20. Nakayama, W. and Torii, T., (1974) "Numerical Analysis of Separative Power of Isotope Centrifuges", J. Nucl. Sci. Technol., 11, 495.

21. Kai, T., (1977) "Basic Characteristics of Centrifuges (IV) - Analysis of Separation Performance", J. Nucl. Sci. and Technol., 14, 506.

22. Furry, W.H., Jones, R.C. and Onsager, L., (1939) "On the Theory of Isotope Separation by Thermal Diffusion", Phys. Rev. 55, 1083.

23. Hogland, R.L., Schachter, J. and Von Halle, E., (1979) "Diffusion Separation Methods", in Encyclopedia of Chemical Technology, Vol. 7, 3rd Ed. R.E. Kirk and D.F. Othmer, Eds., Wiley.

24. May, W.G., (1977) "Separative Parameters of Gas Centrifuges"; AIChE Symp. Ser., No. 169, Vol. 73.

25. Von Halle, E, (1979) "The Optimum Axial Flow Taper in a Countercurrent Gas Centrifuge", U.S. DOE Report K/OA-4445.

26. Soubbaramayer and Billett, J., (1980) "A Numerical Method for Optimizing the Gas Flow in a Centrifuge", Comput. Methods Appl. Mech. and Engin., 24, 165.

Appendix A - Onsager's Master Equation[9]

The starting point for deriving Onsager's equation is the set of linearized conservation equations, which are given by Eqs. (7a) - (7f) of the text. Dropping all terms in these equations which involve axial diffusion of heat and momentum as well as the term representing radial diffusion of radial momentum yields the following set of partial differential equations for the six perturbation variables u, v, w, $\bar{p}$, $\bar{\rho}$, and $\bar{T}$.

$$\frac{1}{r}\frac{\partial}{\partial r}(\rho_{eq} r u) + \frac{\partial}{\partial z}(\rho_{eq} w) = 0 \qquad \text{(mass)} \qquad (A\text{-}1)$$

$$-\bar{\rho} r \Omega^2 - 2\rho_{eq}\Omega v + \frac{\partial \bar{p}}{\partial r} = 0 \qquad \text{(radial momentum)} \qquad (A\text{-}2)$$

$$2\rho_{eq}\Omega u = \mu \frac{\partial}{\partial r}\left[\frac{1}{r}\frac{\partial}{\partial r}(rv)\right] \qquad \text{(azimuthal momentum)} \qquad (A\text{-}3)$$

$$\frac{\partial \bar{p}}{\partial z} = \mu \frac{1}{r}\frac{\partial}{\partial r}\left(r \frac{\partial w}{\partial r}\right) \qquad \text{(axial momentum)} \qquad (A\text{-}4)$$

$$-\rho_{eq}\Omega^2 r u = \kappa \frac{1}{r}\frac{\partial}{\partial r}\left(r \frac{\partial \bar{T}}{\partial r}\right) \qquad \text{(energy)} \qquad (A\text{-}5)$$

$$\bar{\rho} = \left(\frac{M}{RT_o}\right)\bar{p} - \rho_{eq}\left(\frac{\bar{T}}{T_o}\right) \qquad \text{(ideal gas law)} \qquad (A\text{-}6)$$

In these equations, μ and κ are the gas viscosity and thermal conductivity, respectively.

First, use of Eqs. (4) and (5) of the text yields:

$$\rho_{eq}\frac{\partial}{\partial r}\left(\frac{\bar{p}}{\rho_{eq}}\right) = \frac{\partial \bar{p}}{\partial r} - \left(\frac{M\Omega^2 r}{RT_o}\right)\bar{p} \qquad (A\text{-}7)$$

Then $\bar{\rho}$ is eliminated from Eq (A-2) by use of Eq(A-6) and the resulting equation is combined with Eq (A-7) to yield :

$$\frac{1}{r}\ \frac{\partial}{\partial r}\ \left(\frac{\bar{p}}{\rho_{eq}}\right) = \Omega\left[\frac{2v}{r} - \Omega\left(\frac{\bar{T}}{T_o}\right)\right] \qquad (A-8)$$

Taking the derivative of Eq.(A-8)with respect to z and eliminating $\partial \bar{p} / \partial z$ by Eq.(A-4). results in :

$$\Omega\ \frac{\partial}{\partial z}\left[\frac{2v}{r} - \Omega\left(\frac{\bar{T}}{T_o}\right)\right] = \mu\ \frac{1}{r}\ \frac{\partial}{\partial r}\left\{\frac{1}{\rho_{eq}}\ \frac{1}{r}\ \frac{\partial}{\partial r}\left[r\ \frac{\partial w}{\partial r}\right]\right\} \qquad (A-9)$$

A mass flow stream function satisfying Eq.(A-1) is defined by :

$$r\ \rho_{eq} u = -\ \frac{\partial \psi}{\partial z} \qquad (A-10)$$

$$r\ \rho_{eq} w = \frac{\partial \psi}{\partial r} \qquad (A-11)$$

The definition of the stream function is completed by the specification $\psi\ (a,\ z) = 0$, which yields :

$$\psi = -\int_r^a \rho_{eq}\ wr'\ dr' \qquad (A-12)$$

A new quantity χ , called the Master potential, is defined by :

$$\psi = \frac{1}{r}\ \frac{\partial \chi}{\partial r} \qquad (A-13)$$

In terms of χ , the radial and axial mass flows are :

$$r\ \rho_{eq} u = -\ \frac{\partial^2 \chi}{r\ \partial r\ \partial z} \qquad (A-14)$$

and

$$\rho_{eq}\ w = \frac{1}{r}\ \frac{\partial}{\partial r}\ \left(\frac{1}{r}\ \frac{\partial \chi}{\partial r}\right) \qquad (A-15)$$

Taking $\frac{1}{r}\frac{\partial}{\partial r}$ of Eq.(A-9) and using Eq.(A-15) yields :

$$\Omega^2 \frac{\partial^2}{r\,\partial r\,\partial z}\left[\frac{2v}{r\Omega} - \frac{\overline{T}}{T_o}\right] = \mu \frac{\partial^2}{(r\,\partial r)^2}\left\{\frac{1}{\rho_{eq}}\frac{1}{r}\frac{\partial}{\partial r}\left[r\frac{\partial}{\partial r}\left(\frac{1}{\rho_{eq}}\frac{\partial^2 \chi}{(r\,\partial r)^2}\right)\right]\right\} \tag{A-16}$$

where :

$$\frac{\partial^2}{(r\partial r)^2} = \frac{1}{r}\frac{\partial}{\partial r}\left(\frac{1}{r}\frac{\partial}{\partial r}\right) \tag{A-17}$$

The left hand side of Eq.(A-16) can be expressed in terms of axial derivatives of the Master potential by the following arguments.

The first term on the left hand side of Eq.(A-16) is :

$$2\Omega \frac{\partial^2 (v/r)}{r\partial r\partial z} = 2\Omega \frac{\partial}{\partial z}\left[\frac{1}{r}\frac{\partial (v/r)}{\partial r}\right] \tag{A-18}$$

Using the identity :

$$\frac{1}{r^2}\frac{\partial}{\partial r}\left[r^3 \frac{\partial (v/r)}{\partial r}\right] = \frac{\partial}{\partial r}\left[\frac{1}{r}\frac{\partial}{\partial r}(rv)\right]$$

the azimuthal momentum equation, Eq.(A-3), can be written as :

$$2\rho_{eq}\Omega u = \mu \frac{1}{r^2}\frac{\partial}{\partial r}\left[r^3 \frac{\partial (v/r)}{\partial r}\right] \tag{A-19}$$

Multipliying Eq. (A-14)by $2\Omega/r$ and combining with Eq.(A-19) gives :

$$\frac{1}{r}\frac{\partial (v/r)}{\partial r} = -\frac{2\Omega}{\mu r^4}\frac{\partial \chi}{\partial z} \tag{A-20}$$

The second term on the left hand side of Eq.(A-16) is :

$$-\Omega^2 \frac{\partial^2 (\overline{T}/T_o)}{r\partial r\partial z} = -\frac{\Omega^2}{r^2}\frac{\partial}{\partial z}\left[r\frac{\partial (\overline{T}/T_o)}{\partial r}\right] \tag{A-21}$$

The energy equation, Eq. (A-5), is;

$$\rho_{eq}\Omega^2 ru = -\frac{\kappa T_o}{r}\frac{\partial}{\partial r}\left[r\frac{\partial(\bar{T}/T_o)}{\partial r}\right] \qquad (A-22)$$

Multiplying Eq.(A-14) by Ω^2 and combining with Eq.(A-22) gives :

$$r\frac{\partial(\bar{T}/T_o)}{\partial r} = \frac{\Omega^2}{\kappa T_o}\frac{\partial \chi}{\partial z} \qquad (A-23)$$

Substituting Eq.(A-20) into (A-18) and Eq.(A-23) into (A-21) permits the left hand side of Eq.(A-16) to be expressed in terms of the axial second derivatives of the Master potential. Eq.(A-16) becomes :

$$\frac{\partial^2}{(r\partial r)^2}\left\{\frac{1}{\rho_{eq}}\frac{1}{r}\frac{\partial}{\partial r}\left[r\frac{\partial}{\partial r}\left(\frac{1}{\rho_{eq}}\frac{\partial^2\chi}{(r\partial r)^2}\right)\right]\right\} + \frac{1}{\mu}\left[\frac{4\Omega^4}{\mu r^4} + \frac{\Omega^4}{\kappa T_o r^2}\right]\frac{\partial^2\chi}{\partial z^2} = 0 \qquad (A-24)$$

when expressed in dimensionless terms, this is Eq. (9) of the text:

Appendix B - Radial End Mode Solutions

Following Onsager[9], a new radial coordinate is defined by:

$$t = \xi - \ln \lambda \tag{B-1}$$

which transforms Eq. (29) of the text to:

$$\frac{d^2}{dt^2}\left\{ e^t \frac{d^2}{dt^2}\left(e^t \frac{d^2 f^E}{dt^2} \right)\right\} + f^E = 0 \tag{B-2}$$

Being of sixth order, this equation requires six boundary conditions. These are similar to those given in Sect.B.3., except that feed and wall thermal drive effects are neglected ; these have been accounted for in the zero eigenvalue solution. At $\xi = 0$ (or $t = - \ln \lambda$), the boundary conditions for Eq. (B-2) are:

$$f^E_t = f^E_{tt} = L_5 f^E = 0 \quad \text{at } t = - \ln \lambda \tag{B-3}$$

where the subscripts t and tt denote the first and second derivatives, respectively, and L_5 is the operator defined by Eq.(21) (with ξ replaced by t).

Because the radial components of the end modes decrease rapidly with increasing distance from the wall, the boundary conditions at the inner edge of the Stewartson layer are :

$$f^E_t = L_3 f^E = f^E = 0 \qquad \text{at } t = \infty \tag{B-4}$$

Here L_3 is the third order differential operator used on the left and side of Eq (26) of the text, with ξ replaced by t.

Onsager solved Eq (B-2) using the method of Frobenius. He showed that only three of the six solutions satisfy Eq (B-4) The remaining solutions, which we denote by $f_A(t)$, $f_B(t)$ and $f_C(t)$, are infinite series

containing terms which decay exponentially in t. These solutions are given in the paper by Wood and Morton[10], so we do not reproduce them here. The solution of Eq (B-2) can therefore be written as :

$$f^E(t) = \alpha f_A(t) + \beta f_B(t) + \gamma f_C(t) \qquad \text{(B-5)}$$

where α, β and γ are constants of integration. The boundary conditions at the rotor wall ($t = -\ell n\, \lambda$) are satisfied by substituting Eq (B-5) into Eq (B-3) which yields :

$$\begin{aligned} \alpha f_{At} + \beta f_{Bt} + \gamma f_{Ct} &= 0 \\ \alpha f_{Att} + \beta f_{Btt} + \gamma f_{Ctt} &= 0 \\ \alpha L_5 f_A + \beta L_5 f_B + \gamma L_5 f_C &= 0 \end{aligned} \qquad \text{(B-6)}$$

where the subscripts t and tt and the L_5 operator have the same meanings as in Eq (B-3). Being homogeneous, these three linear equations yield nonzero values of the coefficients α, β and γ only for distinct values of λ. Both the coefficients α, β and γ and the eigenvalues λ are obtained by setting the determinant of the matrix formed by the f-functions and their derivatives in Eq(B-6) equal to zero. The roots of this determinant equation are the end mode eigenvalues, denoted by λ_n ($n = 1, 2, 3.....$). Because the equation is homogeneous, the values of α, β and γ which correspond to each eigenvalue are determined only to within an arbitrary multiplicative constant. Accordingly, α can be set equal to unity and the magnitude of the end mode contribution to the Master potential remains to be fixed by coupling the Stewartson layer solution to the Ekman layer solution.

Thus, corresponding to each eigenvalue λ_n there corresponds an eigenfunction $f_n^E(\xi)$ formed by replacing t in the functions on the right hand side of Eq (B-5) by $\xi - \ln \lambda_n$, setting (arbitrarily) $\alpha = 1$, and using the ratios β/α and γ/α calculated from the solution of the determinant equation derived from Eq (B-6) for the λ_n considered.

The first 10 eigenvalues and eigenfunctions for the end modes have been determined in this manner by Morton[16]. Wood and Morton[10] present an asymptotic method of calculating the eigenfunctions and eigenvalues for large n.

Appendix C - The Carrier-Maslen Analysis of the Ekman Layer[10,17]

Because the gradients of velocity in the Ekman layers are primarily in the z-direction, we neglect all radial derivatives in the linearized equations of motion [Eqs (7 b) - (7 e) of the text] are neglected which leaves:

$$-\bar{\rho}\, r\Omega^2 - 2\rho_{eq}\Omega\, v = \mu \frac{d^2 u}{dz^2} \tag{C-1}$$

$$2\rho_{eq}\Omega\, u = \mu \frac{d^2 v}{dz^2} \tag{C-2}$$

$$\frac{d\bar{p}}{dz} = \mu \frac{d^2 w}{dz^2} \tag{C-3}$$

$$-\rho_{eq}\Omega^2\, ru = \kappa \frac{d^2\bar{T}}{dz^2} \tag{C-4}$$

Taking d/dz of Eq. (7f) of the text and replacing $d\bar{p}/dz$ appearing therein with Eq. (C-3) yields:

$$\frac{d\bar{\rho}}{dz} = \left(\frac{M\mu}{RT_o}\right) \frac{d^2 w}{dz^2} - \frac{\rho_{eq}}{T_o} \frac{d\bar{T}}{dz} \tag{C-5}$$

Now take d/dz of Eq (C-1) and eliminate $d\bar{\rho}/dz$ by Eq. (C-5):

$$-\frac{2\rho_{eq}\Omega}{\mu} \frac{d}{dz}\left[v - \frac{r\Omega}{2} \frac{\bar{T}}{T_o}\right] = \frac{d^3 u}{dz^3} + \left(\frac{M}{RT_o}\right)(r\Omega^2) \frac{d^2 w}{dz^2} \tag{C-6}$$

Introduce a nondimensional velocity stream function satisfying Eq (7a) of the text:

$$u = \Omega a^2 \frac{\partial \psi}{\partial z} \tag{C-7}$$

$$r\rho_{eq}w = -\Omega a^2 \frac{\partial}{\partial r}(r\rho_{eq}\Psi) \simeq -\Omega a^3 \frac{\partial}{\partial r}(\rho_{eq}\Psi) \qquad \text{(C-8)}$$

The pancake approximation $r \simeq a$ has been used. Substituting Eqs. (C-7) and (C-8) into Eq. (C-6), dropping r-derivatives and retaining only the highest order derivative of Ψ with respect to z yields:

$$-\frac{2\rho_{eq}}{\mu a^2}\frac{d}{dz}\left[v - \frac{r\Omega}{2}\frac{\bar{T}}{t_o}\right] = \frac{d^4\Psi}{dz^4} \qquad \text{(C-9)}$$

The bracketed term in this equation is expressed as a function of Ψ by dividing Eq (C-2) by μ and subtracting Eq(C-4) (which has been multiplied by $r\,\Omega/2\kappa T_0$) followed by eliminating u by use of Eq (C-7):

$$\frac{d^2}{dz^2}\left[v - \frac{r\Omega}{2}\frac{\bar{T}}{T_o}\right] = \frac{2\Omega^2 a^2 \rho_{eq}}{\mu}\left(1 + \frac{r^2\Omega^2\mu}{4\kappa T_o}\right)\frac{d\Psi}{dz} \qquad \text{(C-10)}$$

The term in parentheses on the right is related to S of Eq (14) of the text. For $r/a \simeq 1$ (the pancake approximation):

$$1 + \frac{r^2\Omega^2\mu}{4\kappa T_o} \simeq S \qquad \text{(C-11)}$$

and the bracketed term on the left of Eq. (C-10) can be expressed in terms of ϕ of Eq. (20) of the text:

$$v - \frac{r\Omega}{2}\frac{\bar{T}}{T_o} \simeq -\frac{1}{2}a\Omega\phi \qquad \text{(C-12)}$$

In terms of ϕ, Eqs (C-9) and (C-10) can be written as:

$$\frac{d^4\Psi}{dz^4} - \frac{e^{-\xi}}{\varepsilon a^3}\frac{d\phi}{dz} = 0 \qquad \text{(C-13)}$$

and

$$\pm\frac{4\,Se^{-\xi}}{a\varepsilon}\frac{d\Psi}{dz} = \frac{d^2\phi}{dz^2} \qquad \text{(C-14)}$$

where ε is the Ekman number [Eq. (8) of the text] and ρ_{eq} has been expressed in terms of the radial scale height variable by Eq. (11). Integration of Eq. (C-14) once (and setting the integration constant equal to zero) and use of this result to eliminate $d\phi/dz$ from Eq. (C-13) gives:

$$\frac{d^4 \Psi}{dy^4} + 4\Psi = 0 \qquad \text{(C-15)}$$

where

$$y = \frac{S^{1/4} e^{-\xi/2}}{a\sqrt{\varepsilon}} z \qquad \text{(C-16)}$$

is a new axial position variable scaled to the thickness of the Ekman layer. Neglecting solutions which grow exponentially in y, the general solution of Eq. (C-15) is:

$$\Psi - \Psi_\infty = e^{-y}(C_1 \cos y + C_2 \sin y) \qquad \text{(C-17)}$$

Since S is of order unity, these equations show that the thickness of the Ekman layer (i.e. $y \simeq 3$) is $\sim 3\sqrt{\varepsilon}\, a$. In Eq. (C-17), Ψ_∞ is the value of the Ekman layer stream function far from the end cap; this quantity must be equated to the value obtained from the Master equation describing the flow in the Stewartson layer. Finally, ϕ can be determined by a second integration of Eq. (C-14):

$$\phi - \phi_\infty = \frac{2 S^{3/4} e^{-\xi/2}}{\sqrt{\varepsilon}} e^{-y}\left[C_1(\cos y - \sin y) + C_2(\cos y + \sin y)\right] \qquad \text{(C-18)}$$

where the integration constant ϕ_∞ is fixed by the angular velocity and temperature perturbations in the Stewartson layer where it joins the Ekman layer.

Conditions imposed on the bottom end cap determine ϕ at $y = 0$ and serve to determine C_1 and C_2 in Eq. (C-17). If drag of the scoop on the gas at the bottom of the centrifuge is simulated by a bottom end cap which is rotating less rapidly than the rotor wall, the angular velocity perturbation v is nonzero at this horizontal surface. In addition, end-cap thermal drive is represented by a nonzero temperature perturbation $\overline{T}$ at the same location. Because these

two parameters appear together in Eq. (C-12), we let ϕ_B denote the specified value of ϕ at y = 0 and Eq. (C-18) becomes:

$$\phi_B - \phi_\infty = \frac{2 S^{3/4} e^{-\xi/2}}{\sqrt{\varepsilon}} (C_1 + C_2) \qquad \text{(C-19)}$$

Similarly, if Ψ_B denotes the stream function on the bottom end cap Eq. (C-17) yields the condition:

$$\Psi_B - \Psi_\infty = C_1 \qquad \text{(C-20)}$$

Finally, the radial velocity u vanishes along the bottom end cap. From Eq. (C-7), this condition is equivalent to $(\partial\Psi/\partial y)_{y=0} = 0$, and, from Eq. (C-17):

$$C_1 = C_2 \qquad \text{(C-21)}$$

Eliminating C_1 and C_2 between Eqs. (C-19) - (C-21) yields Eq. (44) of the text.

Appendix D - The Onsager-Cohen Method of Solving the Diffusion Convection Equation in a Gas Centrifuge

The Onsager-Cohen integral method for solving the diffusion-convection equation is presented for the enriching section of the centrifuge. The analogous equation for the stripping section follows by replacement of x_p by x_w and P by-W.

Integrating the last term of Eq (72) by parts and introducing the flow function of Eq (2) yields :

$$\underset{(C)}{\left[x_p - x(a)\right]} P = -2\pi(\rho D) \underset{(B)}{\int_0^a r \left(\frac{\partial x}{\partial z}\right) dr} - \underset{(A)}{\int_0^a F \left(\frac{\partial x}{\partial r}\right) dr} \qquad (D\text{-}1)$$

The concentration x and the flow function F both depend upon axial position, but this variable has been omitted to keep the notation simple. We consider separately the three terms in Eq (D-1).

The (A) Term

We first multiply Eq (65) by $2\pi r'dr'$, integrate from r_o to r and solve for $\partial x/\partial r$, utilizing the radial boundary condition of Eq (66) in the process. Substituting $\partial x/\partial r$ into the last term of Eq (D-1) yields :

$$(A) = -\frac{\Delta M \Omega^2}{RT_o} \underset{(A_1)}{\int_0^a x(1-x)Fr dr} + \frac{1}{2\pi\rho D} \frac{\partial}{\partial z} \underset{(A_2)}{\int_0^a F \left[2\pi \int_0^r \rho_{eq} w x r' dr'\right] \frac{dr}{r}} \qquad (D\text{-}2)$$

$$- \frac{1}{2\pi} \frac{\partial^2}{\partial z^2} \underset{(A_3)}{\int_0^a F \left[2\pi \int_0^r x r' dr'\right] \frac{dr}{r}}$$

where axial derivatives have been moved through r-integrations because the variation of F and ρ_{eq} w with z are assumed to be of minor significance in this step. Similarly, the inner boundary of the Stewartson layer r_o has been set equal to zero since the flow function is very small for $r < r_o$.

Concentrations can be extracted from the integrals in Eq (D-2) by defining suitability weighted averages. Defining a flow function weighted average concentration $\bar{x}_1$ by :

$$\bar{x}_1(1 - \bar{x}_1) = \frac{\int_0^a x(1-x)Frdr}{\int_0^a Frdr} \tag{D-3}$$

permits the first term to be written as :

$$(A_1) = - \frac{\Delta M \Omega^2}{RT_o} \bar{x}_1 (1-\bar{x}_1) \int_0^a Frdr \tag{D-4}$$

Similarly, for the second term, the following average concentration :

$$\bar{x}_2 = \frac{\int_0^a F \left[2\pi \int_0^r \rho_{eq} w x r' dr'\right] \frac{dr}{r}}{\int_0^a F^2 \frac{dr}{r}} \tag{D-5}$$

yields :

$$(A_2) = \frac{1}{2\pi\rho D} \frac{d\bar{x}_2}{dz} \int_0^a F^2 \frac{dr}{r} \tag{D-6}$$

$\bar{x}_2$ is nearly, but not quite, the flow function squared weighted concentration.

The A_3 term can be written as :

$$(A_3) = - \frac{1}{2} \frac{d^2 \bar{x}_3}{dz^2} \int_0^a r^2 F \frac{dr}{r} \tag{D-7}$$

where $\bar{x}_3$ is the unweighted average :

$$\bar{x}_3 = \frac{2}{a^2} \int_0^a x r dr \qquad \text{(D-8)}$$

The (A_3) term in Eq. (D-2) is smaller than the other two, and was disregarded completely in the original Cohen treatment[6]. However, it can be retained without greatly complicating the analysis. Although Eq (D-7) calls for the unweighted average in the axial second derivative, $\bar{x}_2$ can be used as an approximation. To eliminate the second derivative in Eq (D-7), we take the derivative of Eq (72) and extract x as $\bar{x}_2$:

$$\pi a^2 (\rho D) \frac{d^2 \bar{x}_2}{dz^2} = \left(2\pi \int_0^a \rho_{eq} w r dr \right) \frac{d\bar{x}_2}{dz} = P \frac{d\bar{x}_2}{dz} \qquad \text{(D-9)}$$

Replacing $d^2 \bar{x}_3/dz^2$ in Eq (D-7) by $d^2 \bar{x}_2/dz^2$ and using Eq (D-9) yields :

$$(A_3) = -\frac{1}{2\pi\rho D} \frac{d\bar{x}_2}{dz} \int_0^a FP \left(\frac{r}{a}\right)^2 \frac{dr}{r} \qquad \text{(D-10)}$$

Adding Eqs (D-4), (D-6) and (D-10) gives :

$$(A) = -\frac{\Delta M \Omega^2}{RT_o} \bar{x}_1 (1-\bar{x}_1) \int_0^a F r dr + \frac{d\bar{x}_2/dz}{2\pi\rho D} \int_0^a F\left(F - P \frac{r^2}{a^2}\right) \frac{dr}{r} \qquad \text{(D-11)}$$

The (B) term

Using Eq (D-8), the B term in Eq (D-1) is :

$$(B) = \pi a^2 (\rho D) \frac{d\bar{x}_3}{dz} \qquad \text{(D-12)}$$

The (C) term

Since we are aiming for an axial enrichment equation involving some radially averaged concentration, the wall concentration x(a) in the (C)

term of Eq (D-1) must be expressed in terms of a radially-averaged value of x. To do this, we first need an expression for the radial concentration gradient. Comparison of the (A) term given by Eq (D-11) and its original definition in Eq (D-1) shows that :

$$\frac{\partial x}{\partial r} = - \frac{\Delta M \Omega^2}{RT_o} \bar{x}_1 (1-\bar{x}_1) r + \frac{d\bar{x}_2/dz}{2\pi \rho D} \frac{F - Pr^2/a^2}{r} \qquad \text{(D-13)}$$

This equation differs from the approximate gradient equation in the earlier Cohen analysis [Eq (48) of Ref. 6] in the Pr^2/a^2 term on the right hand side. Since the flow function defined by Eq (2) reduces to the product flow rate P ar r = a, this additional term is required to insure that the correct boundary condition [Eq (66)] is met at the rotor wall.

When integrated from r = r to r = a, Eq (D-13) yields :

$$x = x(a) + \frac{\Delta M \Omega^2 a^2}{2RT_o} \bar{x}_1 (1-\bar{x}_1) \left(1 - \frac{r^2}{a^2}\right) - \frac{d\bar{x}_2/dz}{2\pi \rho D} \int_r^a \left(F - P \frac{r'^2}{a^2}\right) \frac{dr'}{r'} \qquad \text{(D-14)}$$

We now must choose (arbitrarily) a method of radially averaging the concentration. Any of the three radial averages introduced in the treatment of the (A) and (B) terms could conceivably be used. However, if a choice is available, it is preferable to select an average which, at the two ends of the centrifuge, most nearly represents the product and waste compositions. Because the thickness of the Stewartson layer is comparable to the size of sampling port in the top baffle through which the product is removed, it is unlikely that x_p represents the local concentration at the average radial location of the sampling port. Similarly, neither does the scoop at the bottom of the rotor remove gas of a concentration characteristic of a precise radial position. The most reasonable assumption is that the gas removed from the ends of the centrifuge are mass-weighted averages of the radial concentration distributions at the top and the bottom of the Stewartson layer. The natural weighting is based upon the stratification of the gas by the centrifugal force, that is, by the equilibrium radial density distribution of Eq (11). The density-weighted radial average concentration is defined by :

$$\bar{x}_4 = \frac{\int_0^a \exp\left[-A^2\,(1-r^2/a^2)\right]\, x r dr}{\int_0^a \exp\left[-A^2\,(1-r^2/a^2)\right] r dr} \qquad \text{(D-15)}$$

Substituting x from Eq (D-14) into the integral in Eq (D-15) and assuming $A^2 \gg 1$ leads to the following equation for the (C) term in Eq (D-1)

$$(C) = P(x_p - \bar{x}_4) + \left(\frac{\Delta M}{M}\right) \bar{x}_1\,(1-\bar{x}_1)P - \frac{d\bar{x}_2/dz}{2\pi\rho D} P \int_0^a \exp\left[-A^2\left(1-\frac{r^2}{a^2}\right)\right]\left(F - P\,\frac{r^2}{a^2}\right)\frac{dr}{r} \qquad \text{(D-16)}$$

Axial enrichment gradient equations :

When the (A), (B), and (C) terms given above are substituted into Eq (D-1) there results :

$$\pi a^2(\rho D)\,\frac{d\bar{x}_3}{dz} + \frac{d\bar{x}_2/dz}{2\pi\rho D} \int_0^a \left\{F - P\exp\left[-A^2(1-r^2/a^2)\right]\right\}\left[F - P(r^2/a^2)\right]\frac{dr}{r}$$

$$= \frac{\Delta M\,\Omega^2}{RT_o}\,\bar{x}_1(1-\bar{x}_1)\int_0^a \left\{F - P\exp\left[-A^2(1-r^2/a^2)\right]\right\} r dr - P(x_p - \bar{x}_4) \qquad \text{(D-17)}$$

This axial gradient equation contains four radially averaged concentrations, only one of which ($\bar{x}_4$) is arbitrarily chosen. To be usuable, a final approximation must be made, namely :

$$\bar{x}_1 \simeq \bar{x}_2 \simeq \bar{x}_3 \simeq \bar{x}_4 \qquad \text{(D-18)}$$

That is, the distinction between the four averaging methods is disregarded in the Onsager- Cohen method. Three of the average concentrations in Eq

(D-18) are strongly influenced by the radial stratification of the gas and are not too different from each other. The unweighted average, $\bar{x}_3$ however, is significantly larger than the other three. Fortunately, the terms in which $\bar{x}_3$ enters are of minor importance in the overall separation process.

Replacing all radially averaged concentrations by a single quantity x and expressing radial and axial positions in terms of the scale height [Eq(10)] and the dimensionless axial location [Eq. 12], Eq (D-17) reduces to Eq (73).

FIGURE CAPTIONS

1. An early gas centrifuge (courtesy U.S. Departent of Energy).

2. Interior details of a gas centrifuge.

3. Rotor wall and end cap temperatures for thermal drive of a centrifuge.

4. The first four end-mode eigenfunctions and their associated eigenvalues (from Ref. 10).

5. Matching of the Ekman and Stewartson layer solutions at the bottom end cap.

6. Radial shape of the countercurrent in a centrifuge with no scoop and no feed and a wall temperature gradient of -3×10^{-3} K/cm. rotor radius = 9.15 cm ; rotor length = 335 cm ; mean gas temperature = 300 K ; gas pressure at wall = 100 Torr (after Ref. 10).

7. The countercurrent in a scoop-driven centrifuge ; the centrifuge properties are the same as in Fig. 6 except that the rotor wall temperature is uniform ; scoop drive characterized by a disk with the same radius as the rotor but rotating 0.8 % slower than the latter.(Courtesy J. Billet CEA ', calculation performed by the CENTAURE code [19].

8. Contour plot for internal flow optimization of a centrifuge with scoop and wall thermal drives.

9. Axial concentration distribution for a centrifuge with optimized scoop and wall thermal drives.

10. Effect of feed injection point on separative power.

11. Performance function for a centrifuge with axially invariant circulation. Moving upwards, the curves represent throughputs of 25, 50, 75 and 100 mg UF_6/sec.

12. Performance function for a centrifuge driven by a constant wall temperature gradient for two radial velocity shapes. Moving upwards, the curves represent throughputs of 25, 50, 75 and 100 mg UF_6/sec.

13. Performance function of a scoop -driven centrifuge for two axial flow decay lengths. Moving upwards, the curves represent throughputs of 25, 50, 75 and 100 mg UF_6/sec. The nearly vertical lines represent cascade ideality conditions for asymmetric and symmetric cascades with throughputs of 100 mg UF_6/sec per centrifuge.

14. Construction of a centrifuge performance function. Bottom : optimization with respect to internal flow for a particular combination of cut and throughput ; top : the complete performance function.
15. Interstage flow connections for symmetric and asymmetric cascades.

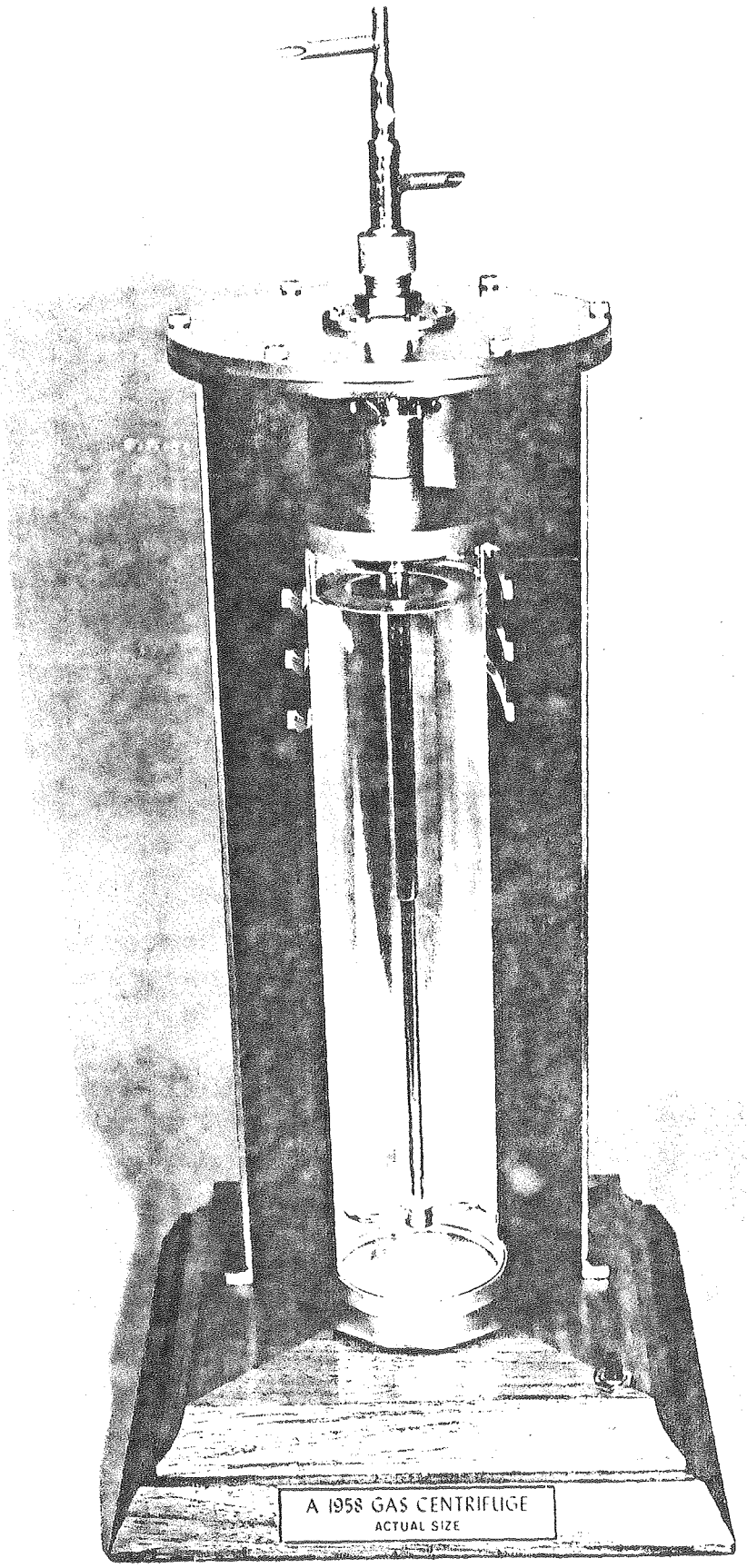

Fig. 1

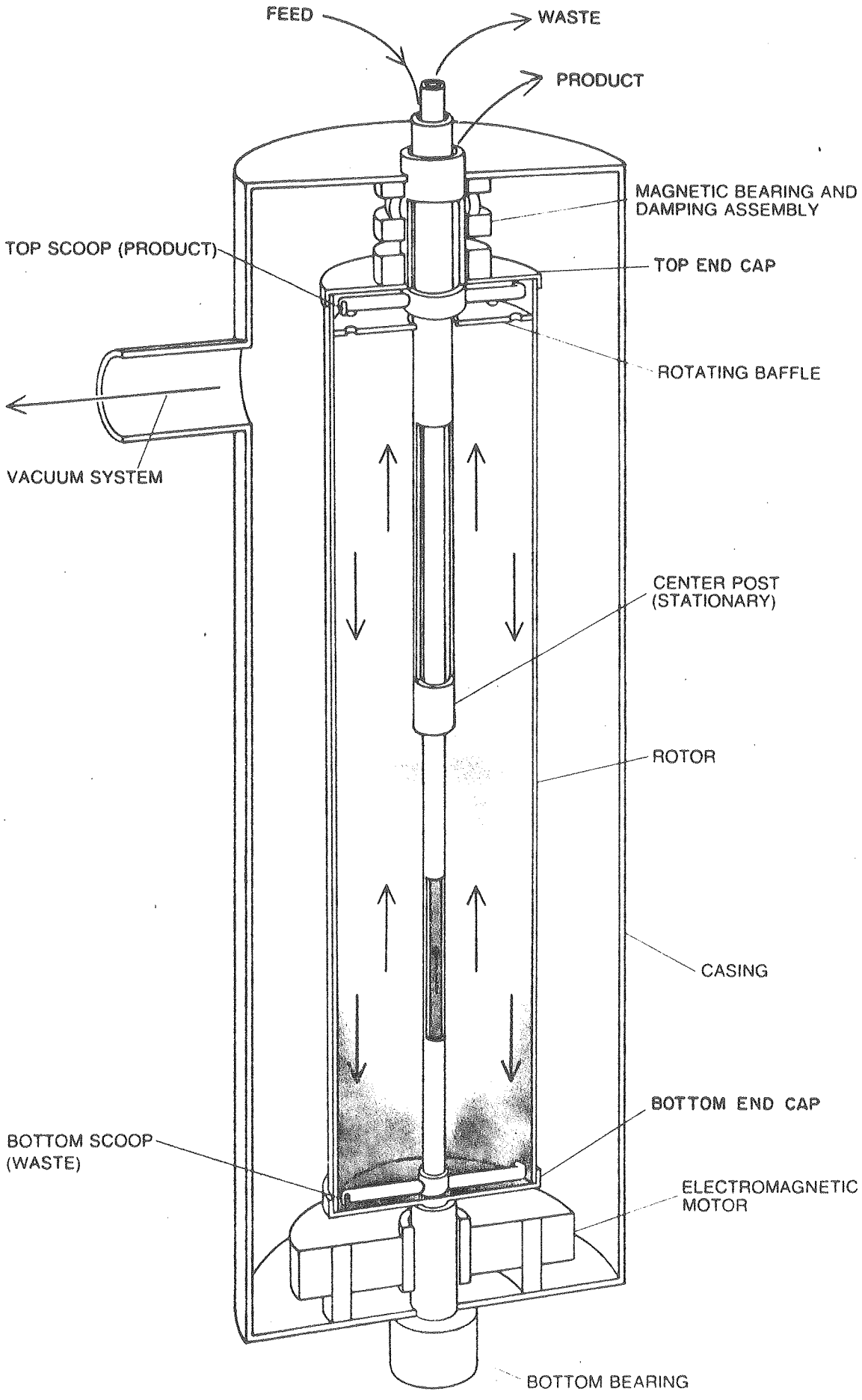

Fig. 2

XBB793-3060A

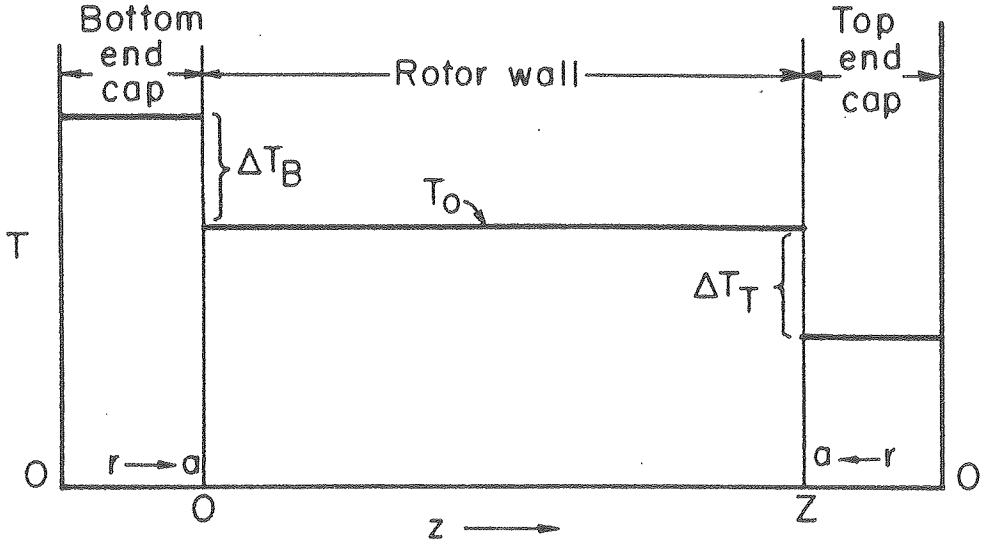

(a) End cap thermal drive

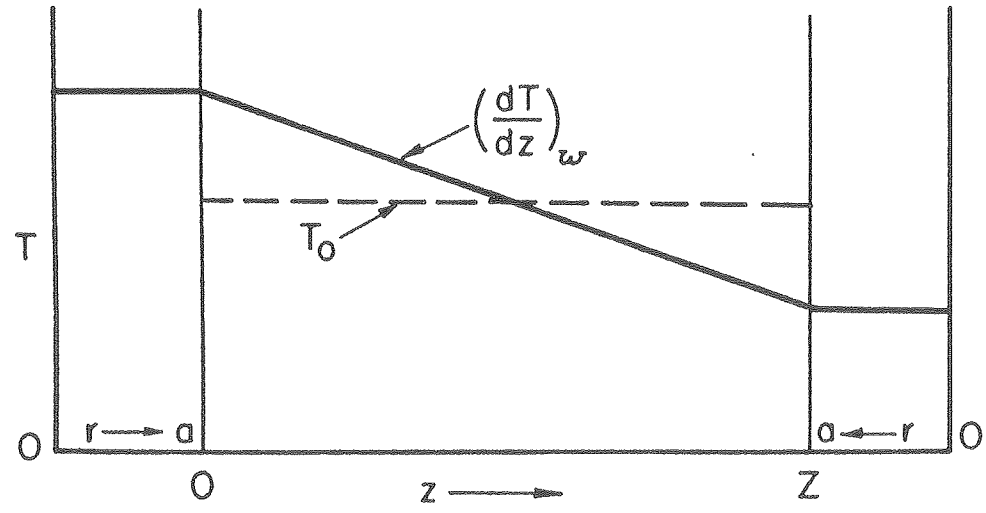

(b) Wall thermal drive

Fig. 3

XBL779-3823

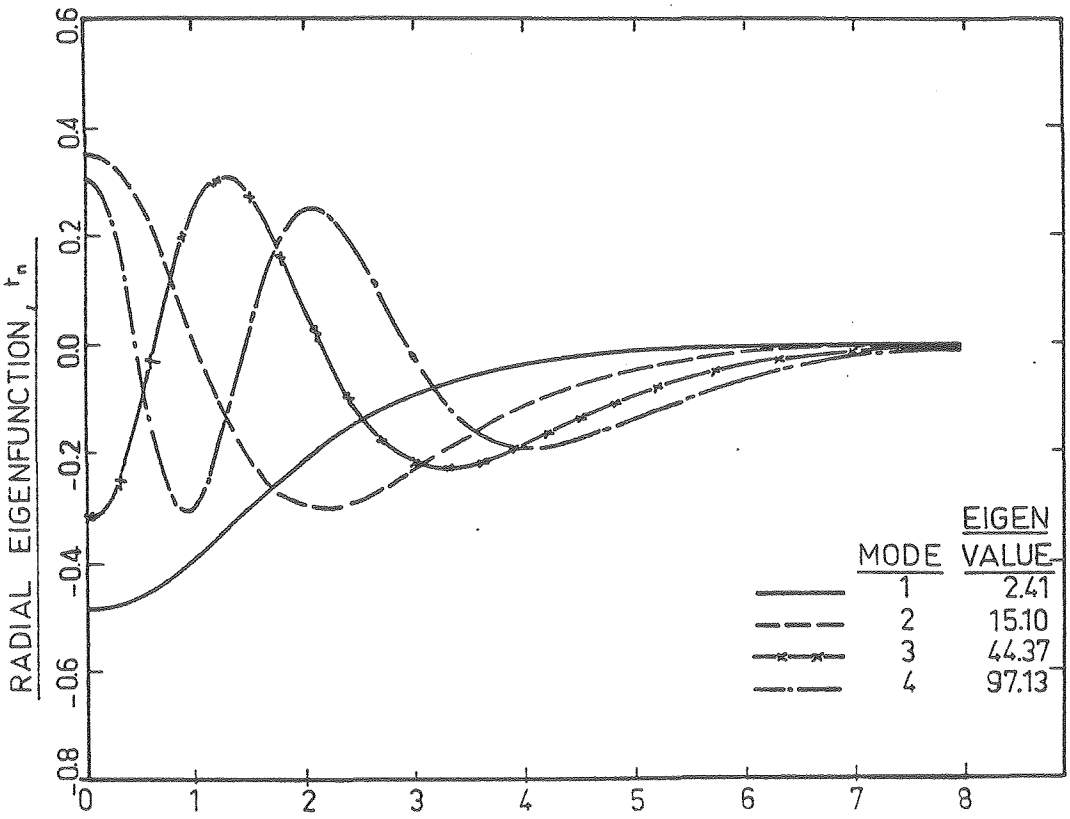
RADIAL EIGENFUNCTION, f_n
0.6
0.4
0.2
0.0
-0.2
-0.4
-0.6
-0.8
0
1
2
3
4
5
6
7
8
EIGEN
MODE VALUE
1 2.41
2 15.10
3 44.37
4 97.13
RADIAL POSITION IN SCALE HEIGHTS ξ

Fig. 4

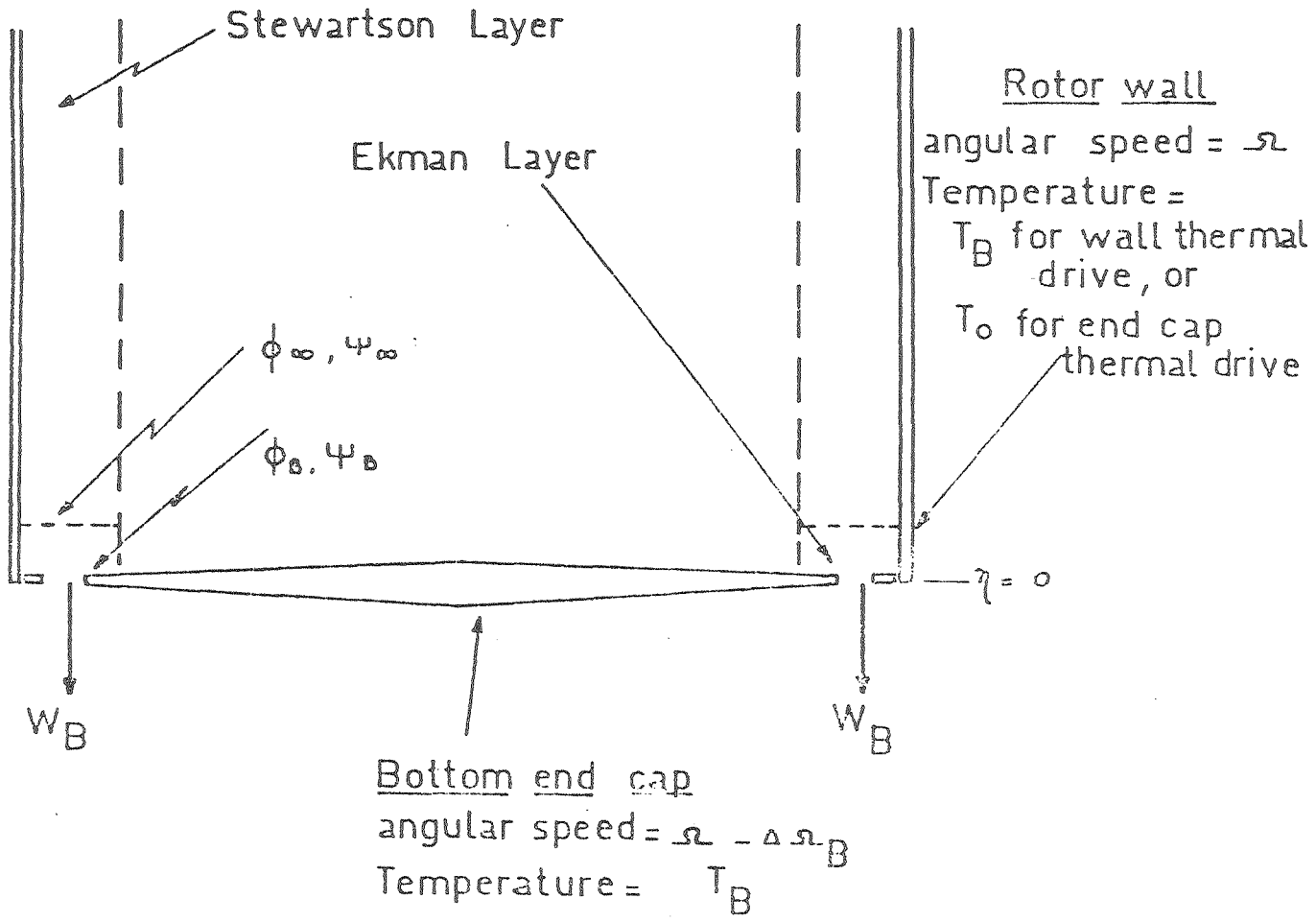
Stewartson Layer
Ekman Layer
Rotor wall
angular speed = Ω
Temperature =
T_B for wall thermal drive, or
T_o for end cap thermal drive
ϕ_∞, ψ_∞
ϕ_B, ψ_B
$\eta = o$
W_B
W_B
Bottom end cap
angular speed = $\Omega - \Delta\Omega_B$
Temperature = T_B

Fig. 5

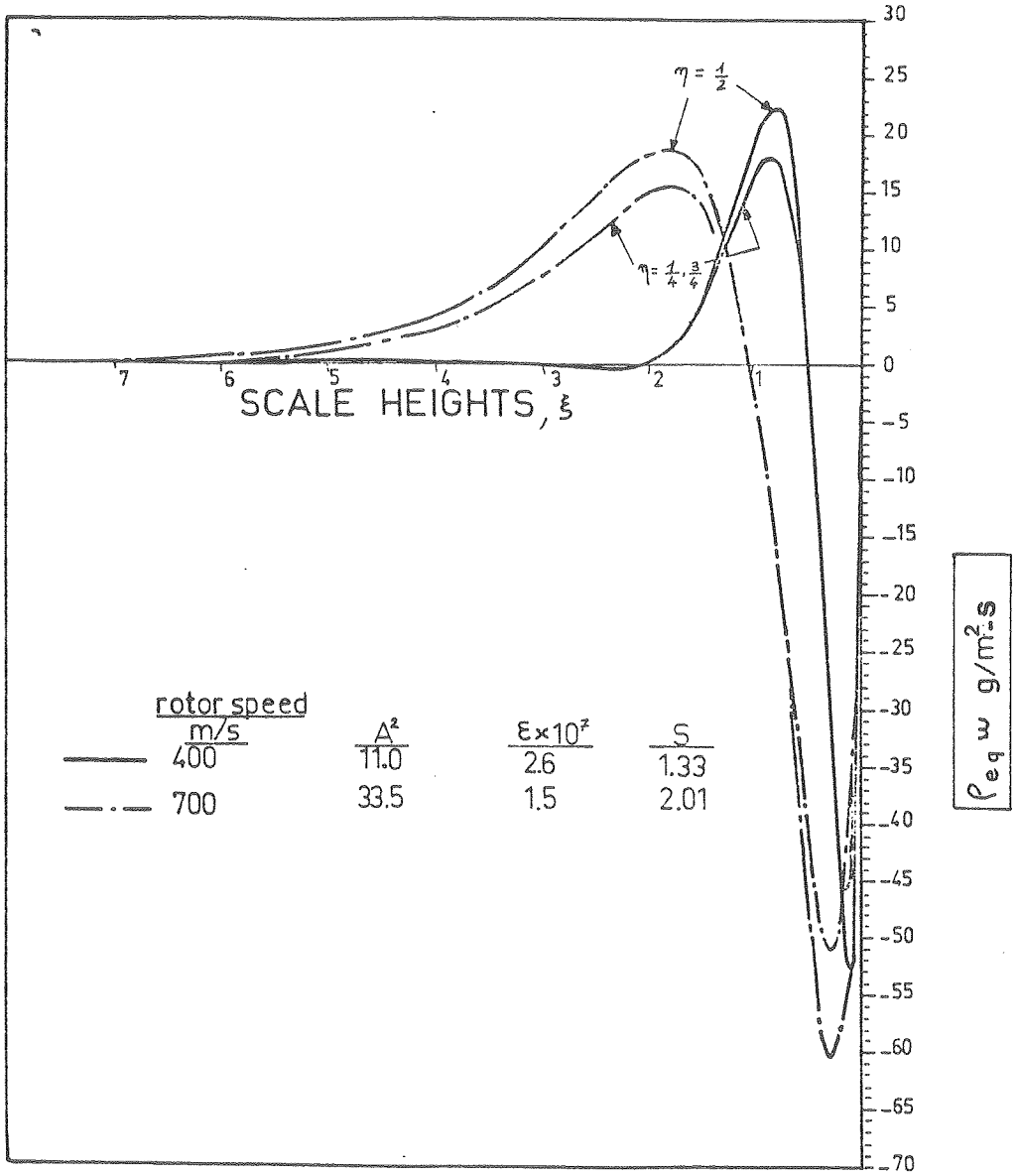
30
25
20
15
10
5
0
-5
-10
-15
-20
-25
-30
-35
-40
-45
-50
-55
-60
-65
-70
$\eta = \frac{1}{2}$
$\eta = \frac{1}{4}, \frac{3}{4}$
7
6
5
4
3
2
1
SCALE HEIGHTS, ξ
rotor speed m/s
A^2
$\varepsilon \times 10^2$
S
400
11.0
2.6
1.33
700
33.5
1.5
2.01
ρ_{eq} w g/m²-s

Fig. 6

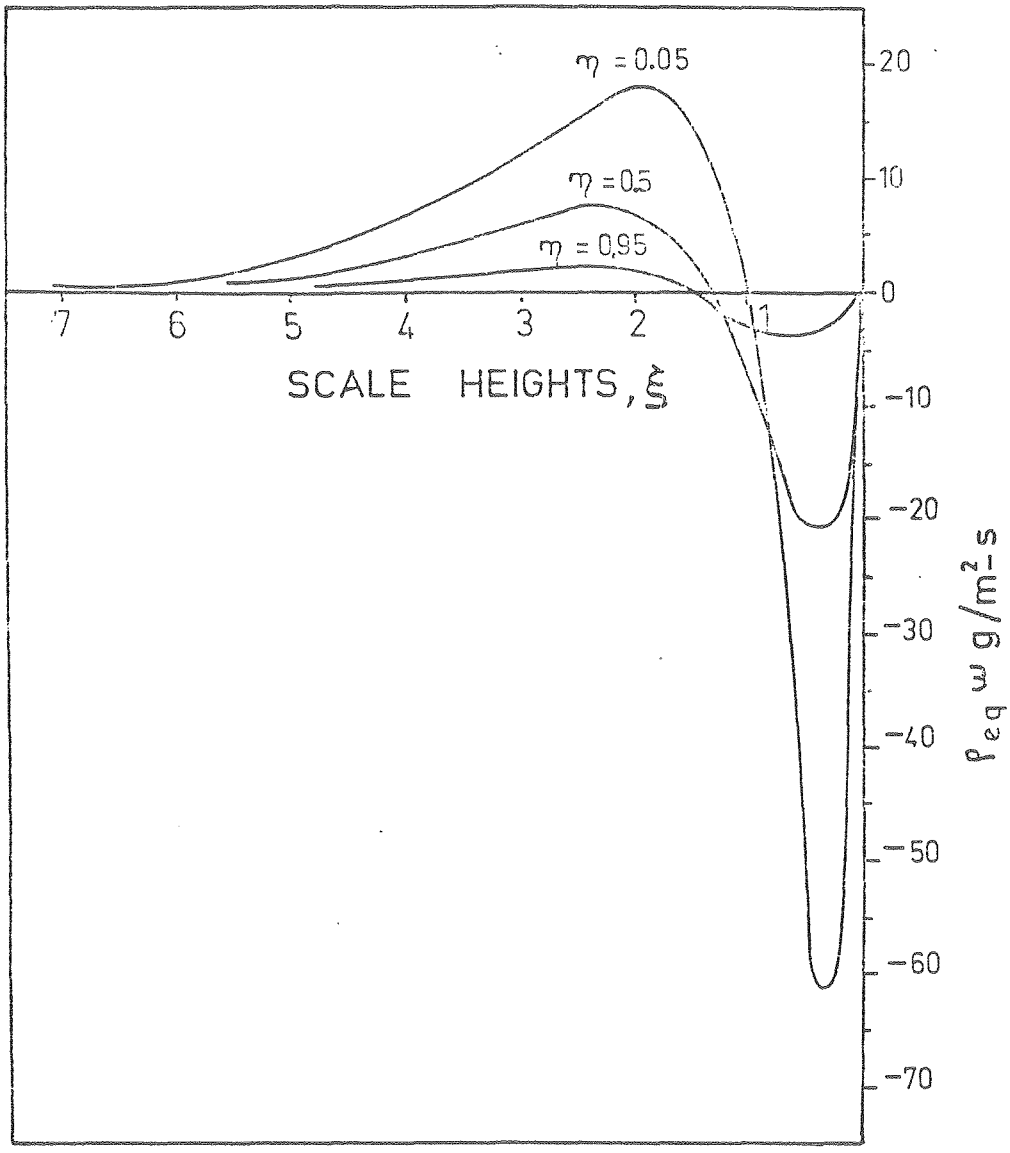
η = 0.05
η = 0.5
η = 0.95
7
6
5
4
3
2
1
SCALE HEIGHTS, ξ
20
10
0
-10
-20
-30
-40
-50
-60
-70
$\rho_{eq}\, w\, g\, /m^2 s$

Fig. 7

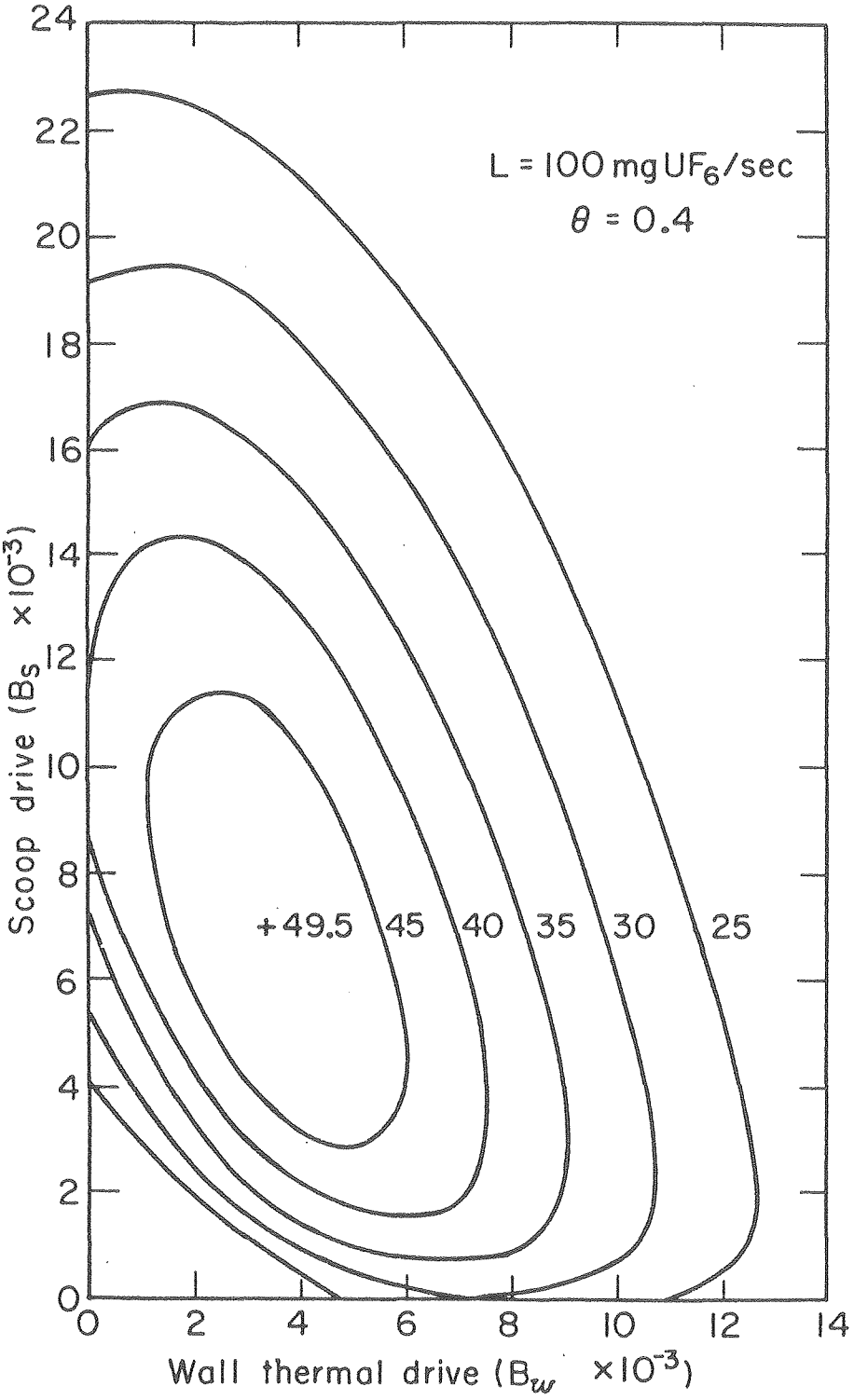

Fig. 8

XBL779-3820

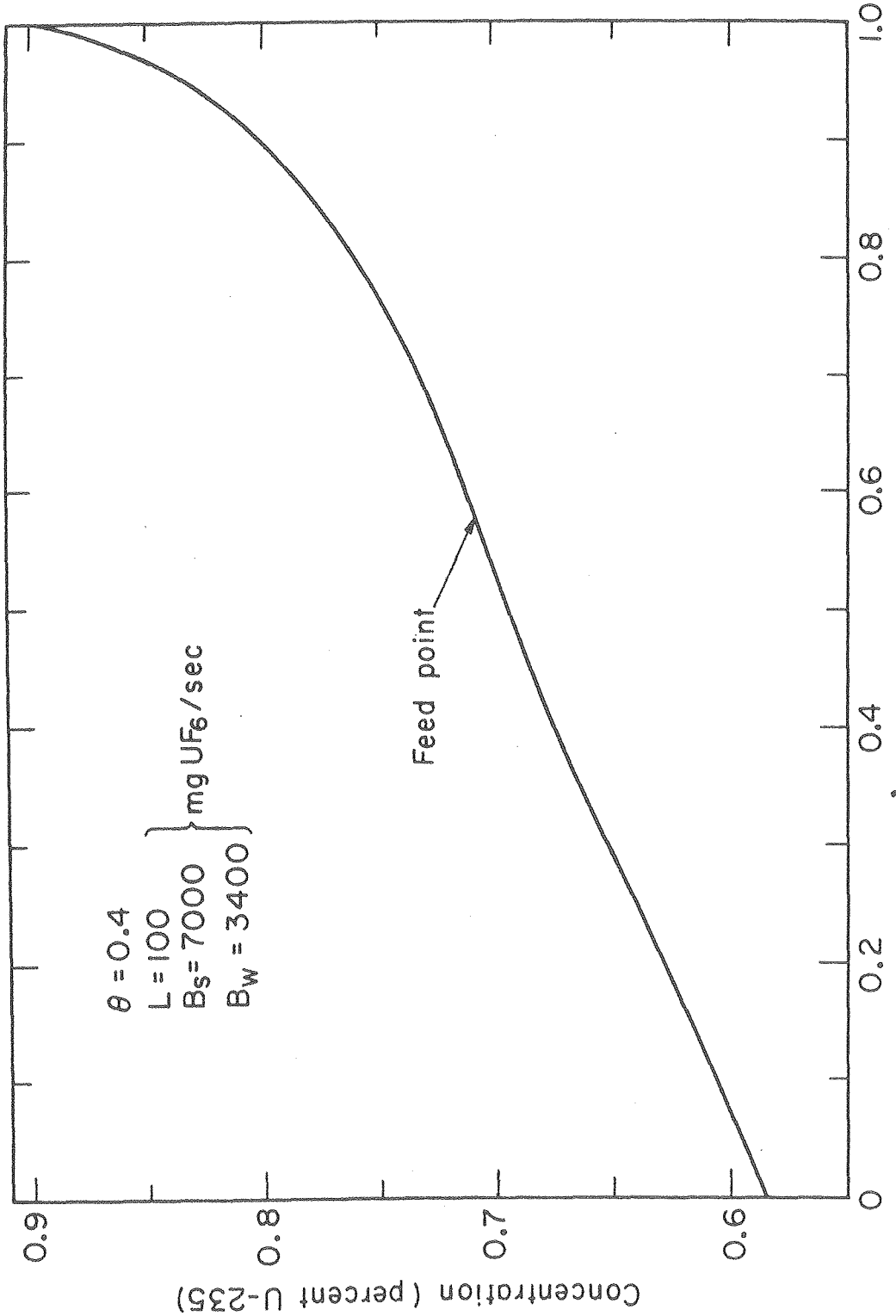
Concentration (percent U-235)
0.9
0.8
0.7
0.6
0
0.2
0.4
0.6
0.8
1.0
Axial position (z/Z)
θ = 0.4
L = 100
Bs = 7000
BW = 3400
mg UF6/sec
Feed point
XBL779-3827

Fig. 9

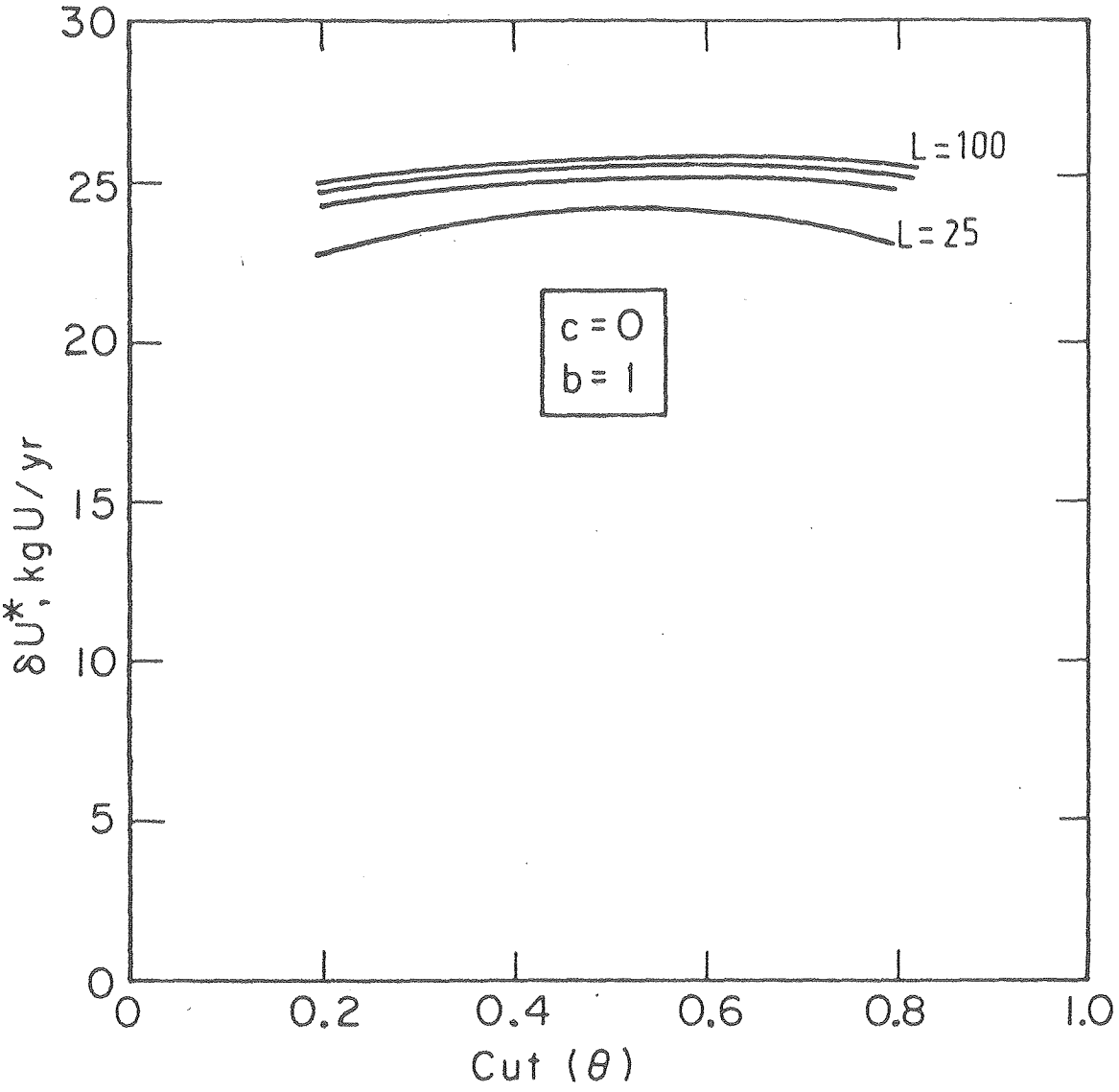

Fig. 10

XBL779-3821

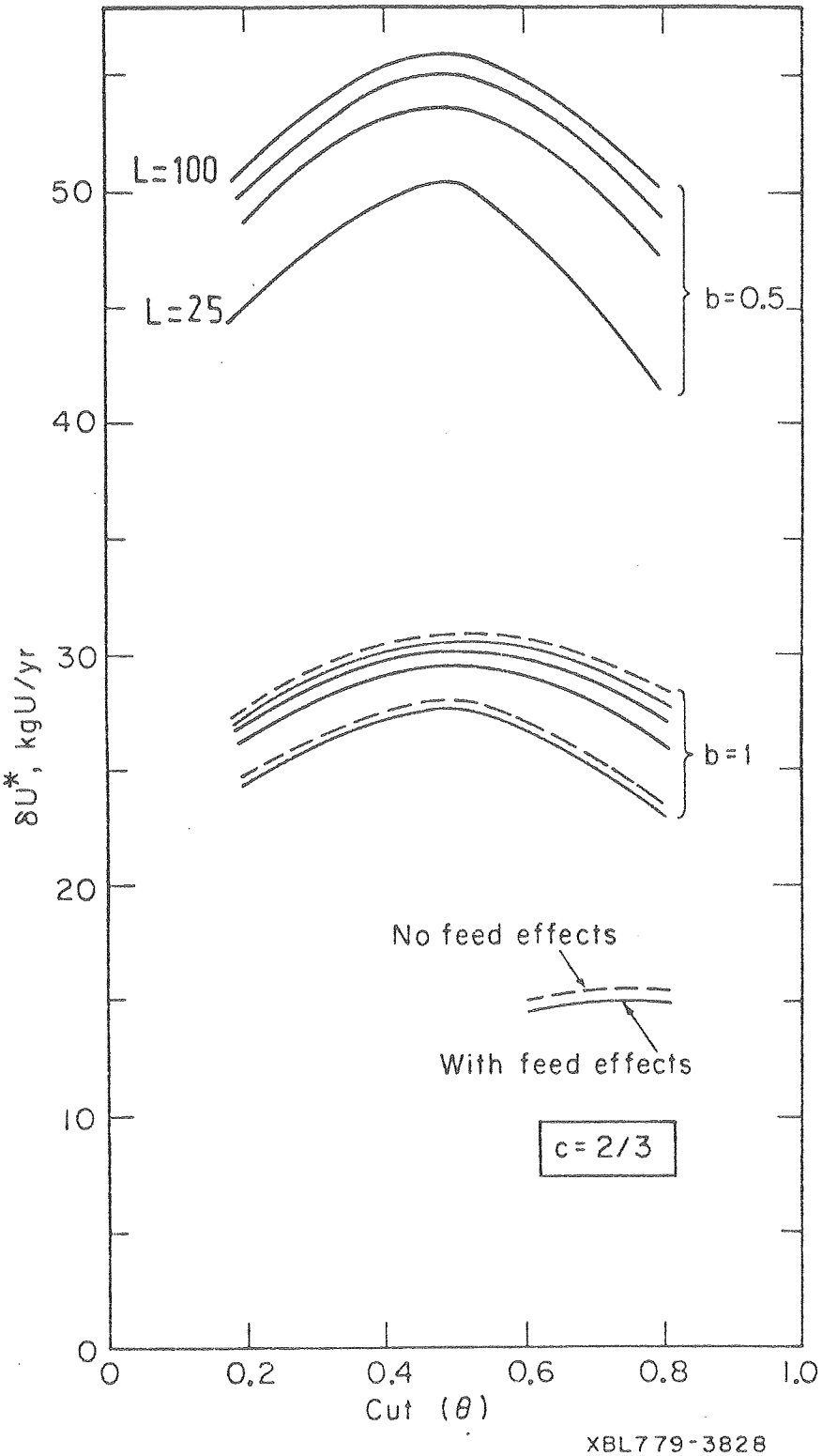
L=100
L=25
b=0.5
b=1
No feed effects
With feed effects
c=2/3
δU*, kgU/yr
Cut (θ)
0
10
20
30
40
50
0.2
0.4
0.6
0.8
1.0
XBL779-3828

Fig. 11

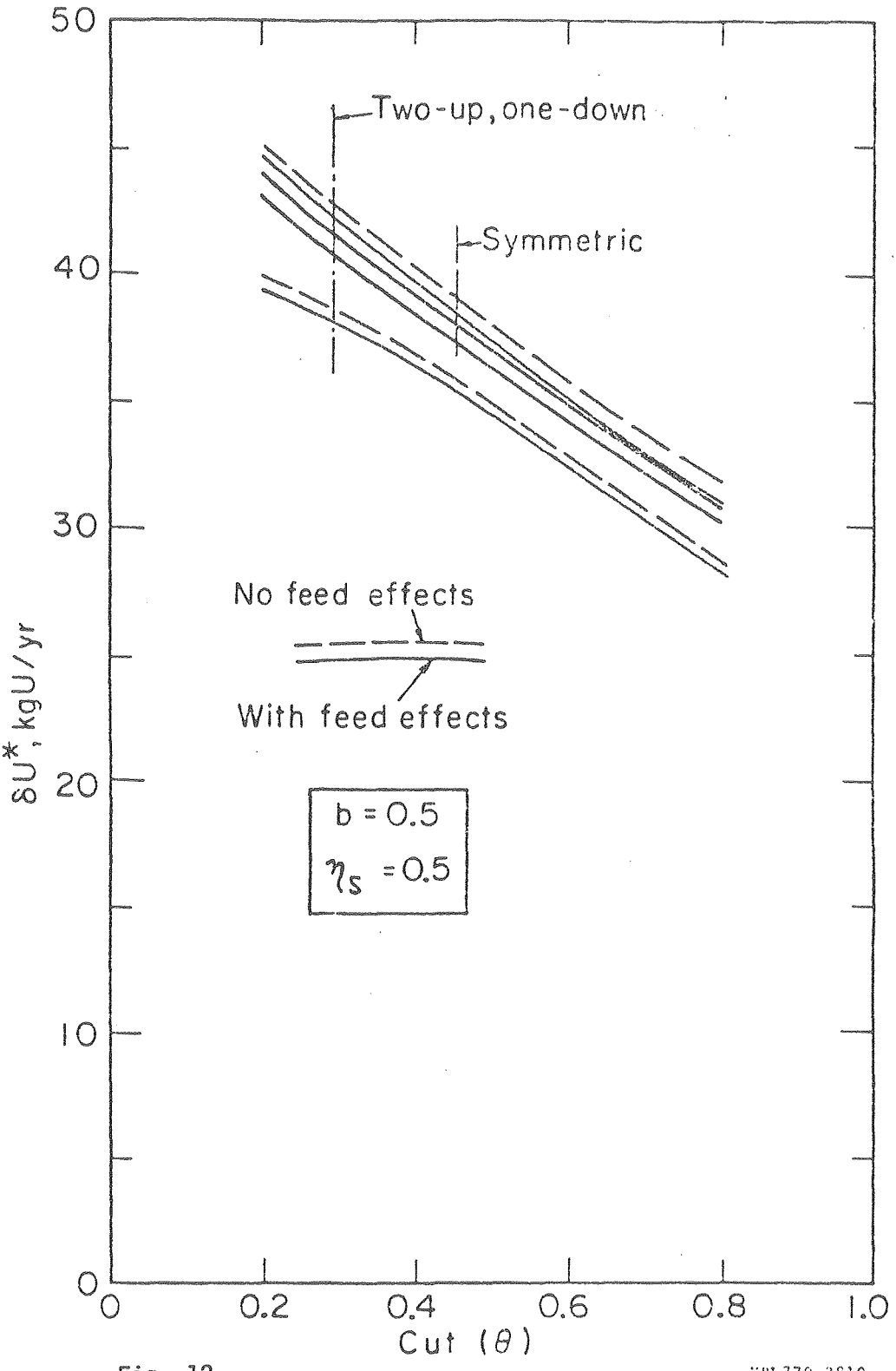

Fig. 12

XBL779-3819

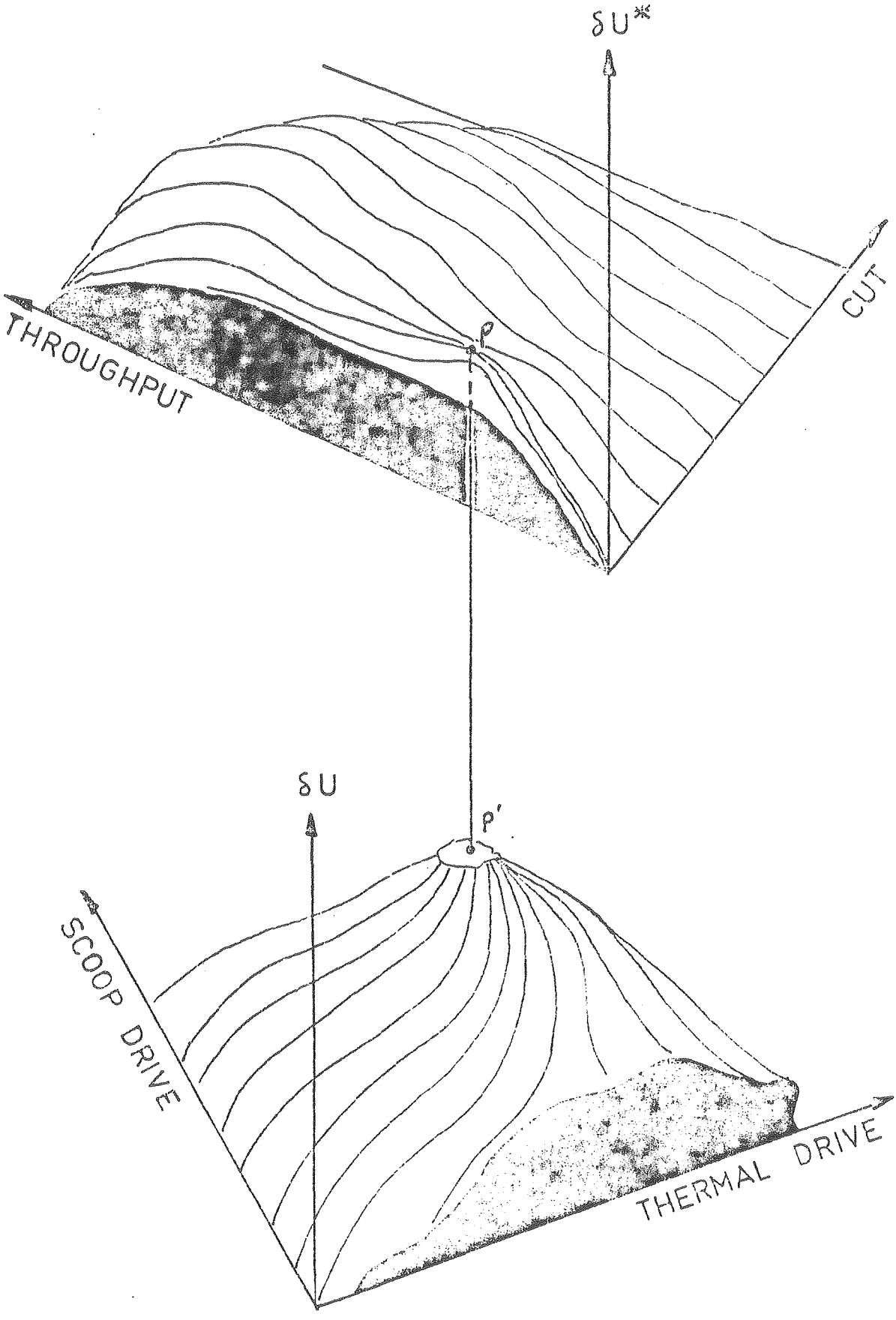

Fig. 13

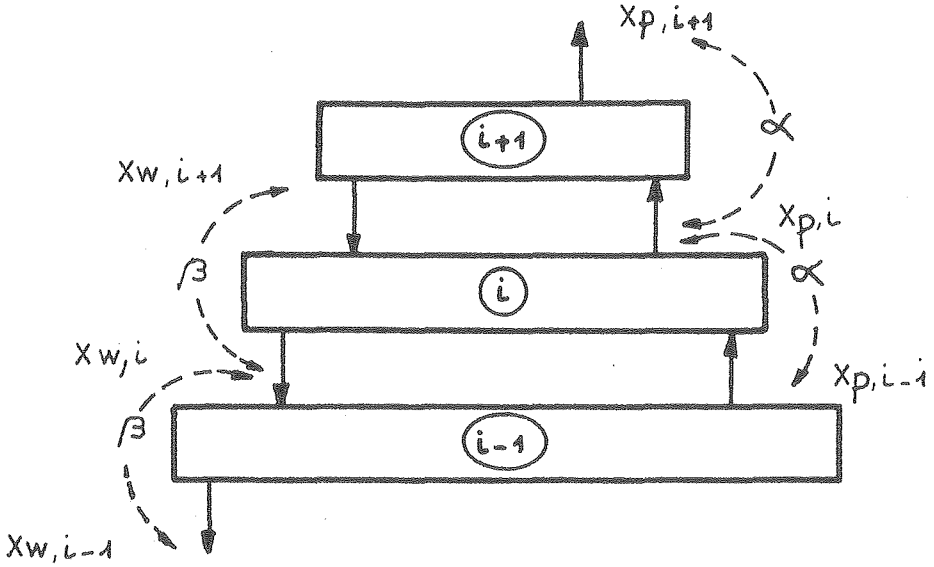

a) Symmetric

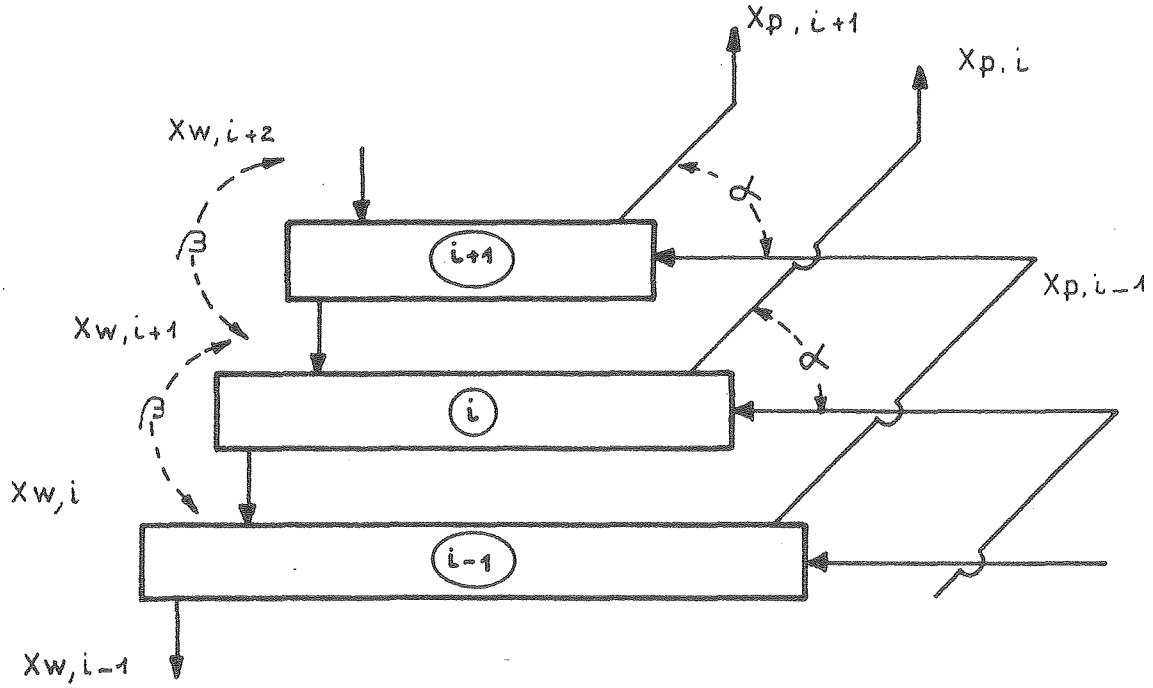

b) Asymmetric (two-up, one-down)

Fig. 14

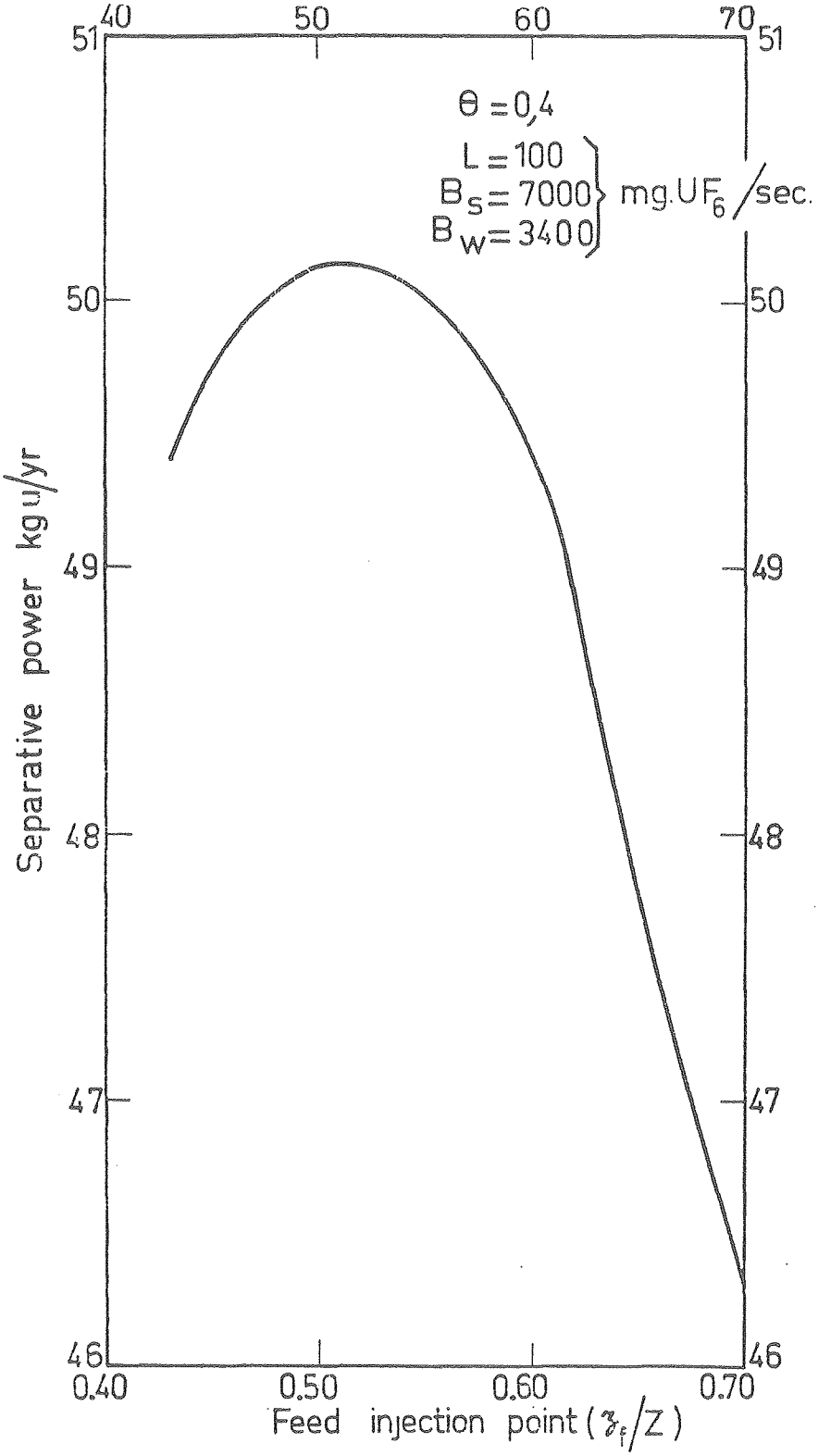
40
50
60
70
51
51
θ = 0,4
L = 100
Bs = 7000
Bw = 3400
mg.UF6 /sec.
50
50
49
49
48
48
47
47
46
46
Separative power kg u/yr
0.40
0.50
0.60
0.70
Feed injection point (zf/Z)

Fig. 15